

NUMERICAL MODELLING OF SATURATED GROUNDWATER FLOW AND POLLUTANT TRANSPORT IN KARST REGIONS

Djoko Luknanto¹

Abstract

In karst regions, groundwater flow and pollutant transport occur in two modes: fast-response flow in cave passages and slow-response flow in the aquifer-matrix. This paper presents, computationally efficient numerical model that simulates the behavior of the two flow and transport modes. First, the fast-response flow in a network of cave passages is mathematically modelled by means of a full unsteady hydrodynamic equation and solved numerically using the Preissmann method. The slow-response flow in the aquifer-matrix is modelled by an unsteady Darcy equation and solved numerically using a fractional-step approach. These two equations are iteratively coupled through an exchange term reflecting the water exchange between cave passages and the aquifer-matrix. Next, the pollutant transport equations in the network of cave passages is solved using a characteristic method and in the aquifer-matrix using a fractional-step approach. These two pollutant transport equations are solved iteratively through an exchange term reflecting the pollutant exchange between cave passages and the aquifer-matrix.

INTRODUCTION

Background

Karst aquifers, in contrast to aquifers in homogeneous media, are extremely complex because of their inhomogeneous permeability. As shown in Figure 1, the relation of structures in rock, such as fracture systems and the orientation of cave passages, establishes secondary permeability. These fractures or cave passages represent less resistance to water flow than does neighboring rock. In contrast to aquifers in homogeneous media, karst aquifers, due to their inhomogeneous distribution of permeability, are extremely complex.

Groundwater flow occurs in two modes: fast-response flow in cave passages and slow-response flow in the aquifer-matrix. These two components of groundwater flow are extremely different in the effectivity of groundwater transmission and groundwater storage. These flow characteristics therefore greatly influence pollutant transport in such a region.

Although unsaturated cases are common in the real world, understanding the behavior of saturated groundwater flow is a very important step toward understanding unsaturated cases. Insight from saturated cases can be applied to the study of unsaturated cases. Study of the physical behavior of saturated cases is, therefore, the beginning of on-going research in groundwater flow in karst regions.

Objective

The objective of the present study is to model the behavior of saturated groundwater flow and pollutant transport in karst regions. A new approach is introduced in which the

⁽¹⁾ Djoko Luknanto, a faculty member of College of Engineering, Civil Engineering Department, Gadjahmada University, Yogyakarta, Indonesia

“full” hydrodynamic equation in a cave passage network is solved directly. The pollutant assumed here is a nonreactive, conservative one, meaning that during transport, its quantity does not increase or decrease. As in any study of groundwater flow, little data are available. This is understandable due to the difficulties in measuring soil parameters, initial and boundary conditions, as well as the high cost involved in obtaining the data. For the purpose of the present study, no new field measurements have been performed. The study uses data obtained from competent published sources.

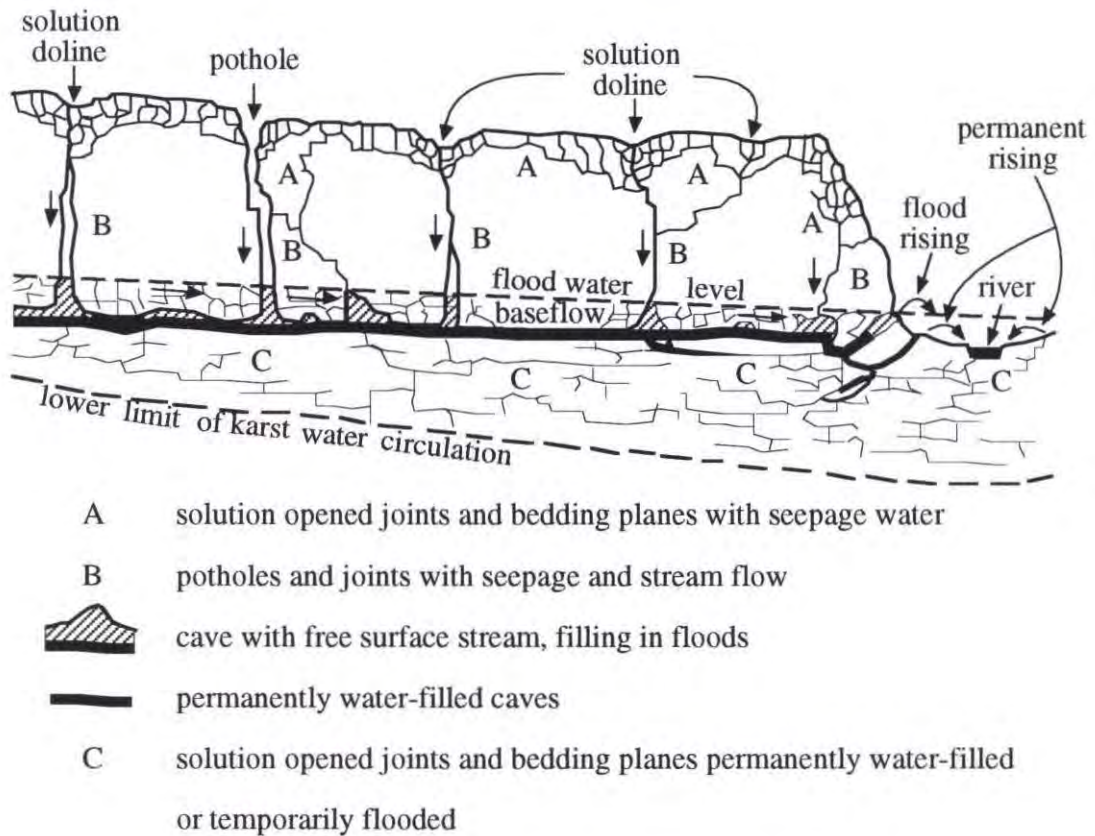


Figure 1. A Karst Hydrologic System Based on the Concept of Independent Conduits, after Cavaille (1962)

It is very important to mention that the present study is part of a larger research objective; i.e., the present study serves as the deterministic part of a Monte Carlo simulation of water resources in a karst region. Since available observations are limited, system parameters (aquifer properties, system geometry, initial and boundary conditions) must be generated by statistical techniques. Each realization of the data generated becomes the input data for the “deterministic engine” which processes the data to produce one realization of output. In a Monte Carlo simulation, hundreds or thousands of realizations of input may be generated, each of which produces its corresponding output. These in turn must be interpreted by statistical means. In karst regions, the “deterministic engine” will be a model that simulates numerically the behavior of groundwater water and pollutant transport for unsaturated cases. Since the present study is only capable of handling saturated cases, it must be extended to unsaturated cases in order to become the complete “deterministic

engine” for the Monte Carlo simulation.

The topology of cave passages and the boundary of the groundwater flow region are inferred from data obtained for karst formations in the Big Spring Basin, a 103 square mile groundwater basin located in Clayton County, northeastern Iowa (Hallberg et al., 1989), see Figure 2. The topography of the region under study is extracted from the USGS (United States Geologic Survey) contour map. Soil parameters, i.e., hydraulic conductivity, specific storage, exchange coefficient, dispersion coefficient, and effective porosity are based on appropriate published literature.

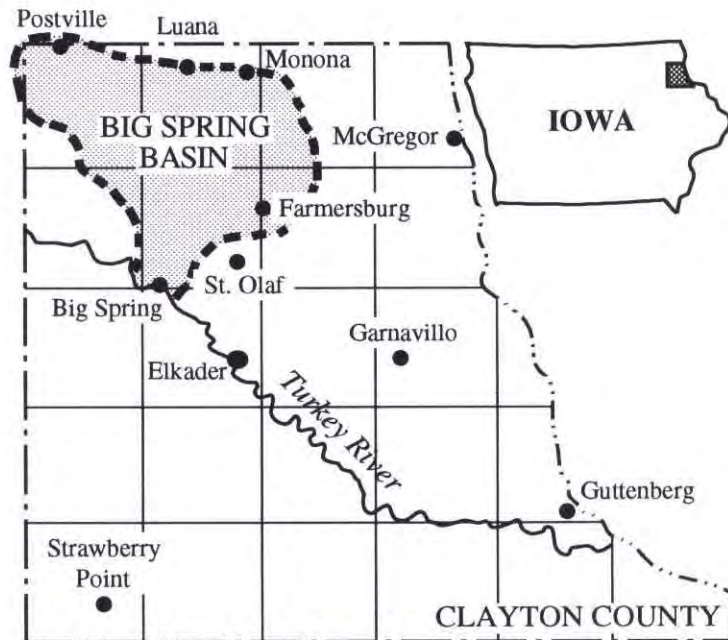


Figure 2. The Big Spring Basin in Clayton County, northeast Iowa, after Hallberg et al. (1989)

MODEL DEVELOPMENT

Introduction

The present study presents a model to simulate a complex, real-life situation. The domain of the model is based on the geometry and topography of the Big Spring Basin, depicted in Figure 4. The domain is three-dimensional, and certain topological conventions are required to handle it. To this end, a so-called “soil-topology” convention has been developed which makes it possible to describe any kind of three-dimensional boundary. All numerical approximations of the governing equations are applied within this topology. In the present study, the finite-difference method is used to approximate the governing equations, and the solution grid is generated to conform as closely as possible to the aquifer topography.

Governing Equations

This section describes all the governing equations used in the present study: hydrodynamic equations, equations of pollutant transport, and mass exchange equations for both the aquifer-matrix and megapore network.

Hydrodynamic Equation for Aquifer-Matrix

The governing equation of flow in porous media is derived from the mass conservation law applied to a control volume.

$$\Delta x \frac{\partial}{\partial x} \left(A_x K_x \frac{\partial h}{\partial x} \right) + \Delta y \frac{\partial}{\partial y} \left(A_y K_y \frac{\partial h}{\partial y} \right) + \Delta z \frac{\partial}{\partial z} \left(A_z K_z \frac{\partial h}{\partial z} \right) - W = S v \frac{\partial h}{\partial t} \tag{1}$$

where K is hydraulic conductivity (LT^{-1}); h is piezometric head (L); W is volumetric source flux (L^3T^{-1}); S is specific storage (L^{-1}); A is cross sectional area of aquifer in each direction, in a finite-difference block (L^2); Δ is the length of control volume in each direction (L); and

$$W = w v \tag{2}$$

In Eq. (2) w is the source term, volumetric flux per unit volume (T^{-1}); and v is the volume of the aquifer in a finite-difference block (L^3). Volumetric flux, W , is the source exchange term between the aquifer-matrix and megapores.

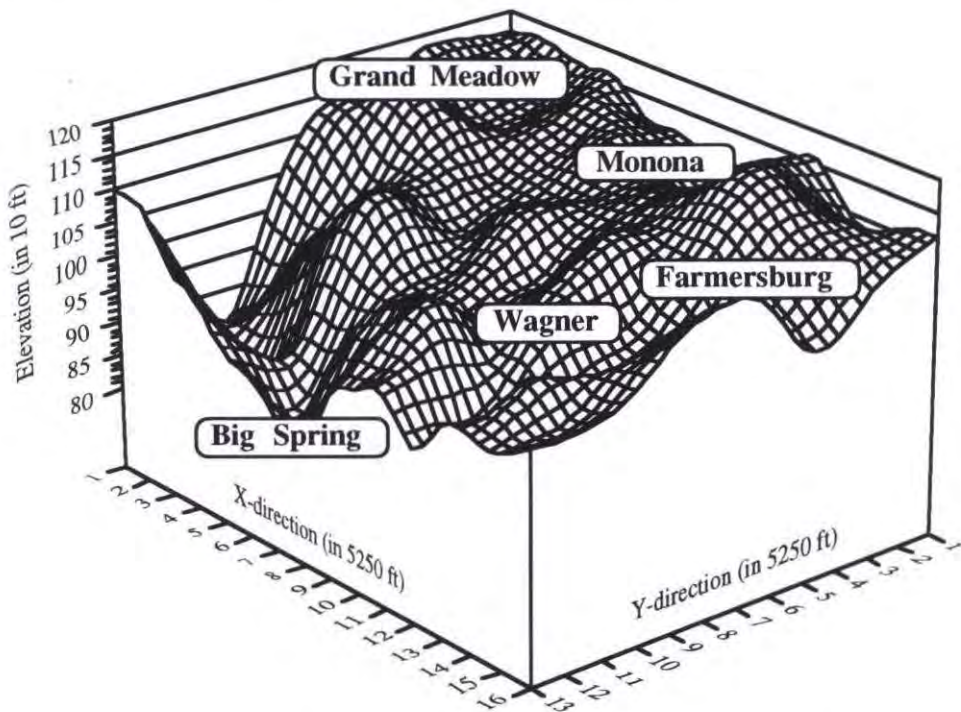


Figure 4. Southeast View of the Big Spring Basin (Iowa, USA)

Pollutant Transport Equation for Aquifer-Matrix

The governing equation of pollutant transport in porous media is also derived from the mass conservation law applied to a control volume. For a nonhomogeneous, anisotropic porous medium, the governing equation can be written in terms of concentration (C) as

$$\Delta x \frac{\partial}{\partial x} \left(A_x D_x \frac{\partial C}{\partial x} \right) + \Delta y \frac{\partial}{\partial y} \left(A_y D_y \frac{\partial C}{\partial y} \right) + \Delta z \frac{\partial}{\partial z} \left(A_z D_z \frac{\partial C}{\partial z} \right) - \Delta x \frac{\partial}{\partial x} (A_x U_x C) - \Delta y \frac{\partial}{\partial y} (A_y U_y C) - \Delta z \frac{\partial}{\partial z} (A_z U_z C) - C_s W = v \frac{\partial C}{\partial t} \quad (3)$$

where $U_x = \frac{-K_x}{e} \frac{\partial h}{\partial x}$ $U_y = \frac{-K_y}{e} \frac{\partial h}{\partial y}$ $U_z = \frac{-K_z}{e} \frac{\partial h}{\partial z}$ $W = v \frac{\partial C}{\partial t}$ (4)

In Eq. (3) C is solute concentration (ML^{-3}); D is the dispersion coefficient (L^2T^{-1}); U is seepage or average pore water velocity (LT^{-1}); C_s is solute concentration in the sources or sinks (ML^{-3}); e is effective porosity; and U_x , U_y , U_z and W are known quantities from the hydrodynamic computation.

Hydrodynamic Equation for Megapores

In the present study, the flow is restricted to one-dimensional, incompressible, full-megapore flow, the principal implication of which is that the discharge in a single megapore must at any instant be constant along its length. Of course the discharge may vary from one megapore to another along a series of megapores in a network due to external or aquifer-matrix inflow. From the law of conservation of momentum, the governing equation in any single megapore can be written as

$$\frac{\partial Q}{\partial t} + \frac{\partial}{\partial s} \left(\frac{Q^2}{A} \right) + gA \left(\frac{\partial h}{\partial s} + S_f \right) = 0 \quad (5)$$

Since $Q \neq Q(s)$ along a megapore, Eq. (5) can be rewritten as

$$\frac{\partial Q}{\partial t} - \left(\frac{Q}{A} \right)^2 \frac{\partial A}{\partial s} + gA \left(\frac{\partial h}{\partial s} + \frac{Q|Q|}{K^2} \right) = 0 \quad (6)$$

where t is time; s is the longitudinal megapore coordinate; Q(t) is megapore discharge; A(s) is megapore cross-sectional area; h(s,t) is the megapore piezometric head; $S_f(s,t)$ is megapore energy slope ($= \frac{Q|Q|}{K^2}$); K(s) is full-megapore conveyance; and g is gravitational acceleration. In Eq. (6), the four terms are associated with local acceleration, advective acceleration, net normal pressure force, and boundary shear force, respectively.

Pollutant Transport Equation for Megapores

The governing equation for pollutant transport can be derived from the law of mass conservation, with the same assumptions as those used to derive hydrodynamic equation. Following the derivation given by Fischer et al. (1979), the pollutant transport equation can

be generalized as

$$\frac{\partial(AC)}{\partial t} + \frac{\partial(AUC)}{\partial s} = \frac{\partial(A \epsilon \frac{\partial C}{\partial s})}{\partial s} \quad (7)$$

Differentiating the left hand side of Eq. (7) and recognizing that $\frac{\partial A}{\partial t} + \frac{\partial(AU)}{\partial s} = 0$ from conservation of mass, Eq. (7) can be rewritten as

$$A \frac{\partial C}{\partial t} + AU \frac{\partial C}{\partial s} = \frac{\partial(A \epsilon \frac{\partial C}{\partial s})}{\partial s} \quad (8)$$

where $U(s,t)$ is velocity of megapore flow, and $\epsilon(s)$ is the megapore dispersion coefficient.

Mass Exchange Between Aquifer-Matrix and Megapores

The mass exchange between aquifer and megapores consists of two constituents, water discharge and pollutant flux. The water discharge exchange uses the same principle used in computing leakage through a semipermeable layer from an overlying (or underlying) aquifer into another aquifer with a different piezometric head (see Bear, 1979, page 36). Therefore, the amount of mass exchange can be computed as a linear function of the difference between the piezometric head inside the megapore and that of the aquifer-matrix surrounding the megapore. The equation of water discharge exchange can be written as

$$w = \alpha (h_s - h_p) \quad (9)$$

where α is the coefficient of exchange ($L^{-1}T^{-1}$); h_s is the piezometric head of the aquifer-matrix (L); and h_p is the piezometric head of the megapore (L).

For the pollutant flux exchange term the assumption is that the advective exchange term is dominant compared to that of the diffusive one. The equation for the pollutant exchange term thus becomes simply the concentration of pollutant in water multiplied by its water discharge:

$$w_s = C_s w \quad (10)$$

where w is as defined in Eq. (9).

Topological Structure of the Aquifer

The aquifer is represented by a three-dimensional block of computational grid points, referred to herein as *aquifer-matrix grid points*. The three-dimensional equations for aquifer-matrix water and pollutant movement are solved numerically on this computational grid.

Preferential flow paths, such as root-zone macropores or karst megapores, are represented as an interconnected network of so-called *pipes*, within which water and pollutant transport are represented as equivalent to flow in full pipes.

Exchange of water and pollutant between the aquifer-matrix and megapore passages is taken to occur only at aquifer-matrix grid points through which the pipe network passes; these intersections are called *nodes*. Thus, it is presumed that however the pipe network is generated (e.g., manually, through stochastic simulation, etc.), it is constrained to pass frequently through aquifer-matrix grid points; i.e., that nodes occur as densely as possible.

Figure 5 is a schematic depiction of a possible simple topological structure. The aquifer-matrix grid point coordinates of nodes are shown in parentheses. Nodes 1, 6, 12, 20, and 33 (shown as inverted triangles) represent intersections of the megapore structure with the ground surface; i.e., sinkholes. Nodes 5, 8, 16, and 23 are junctions of multiple pipe-network flow paths. Nodes 11, 19, 32, and many others not shown, represent aquifer-matrix grid points through which pass a single pipe-flow path.

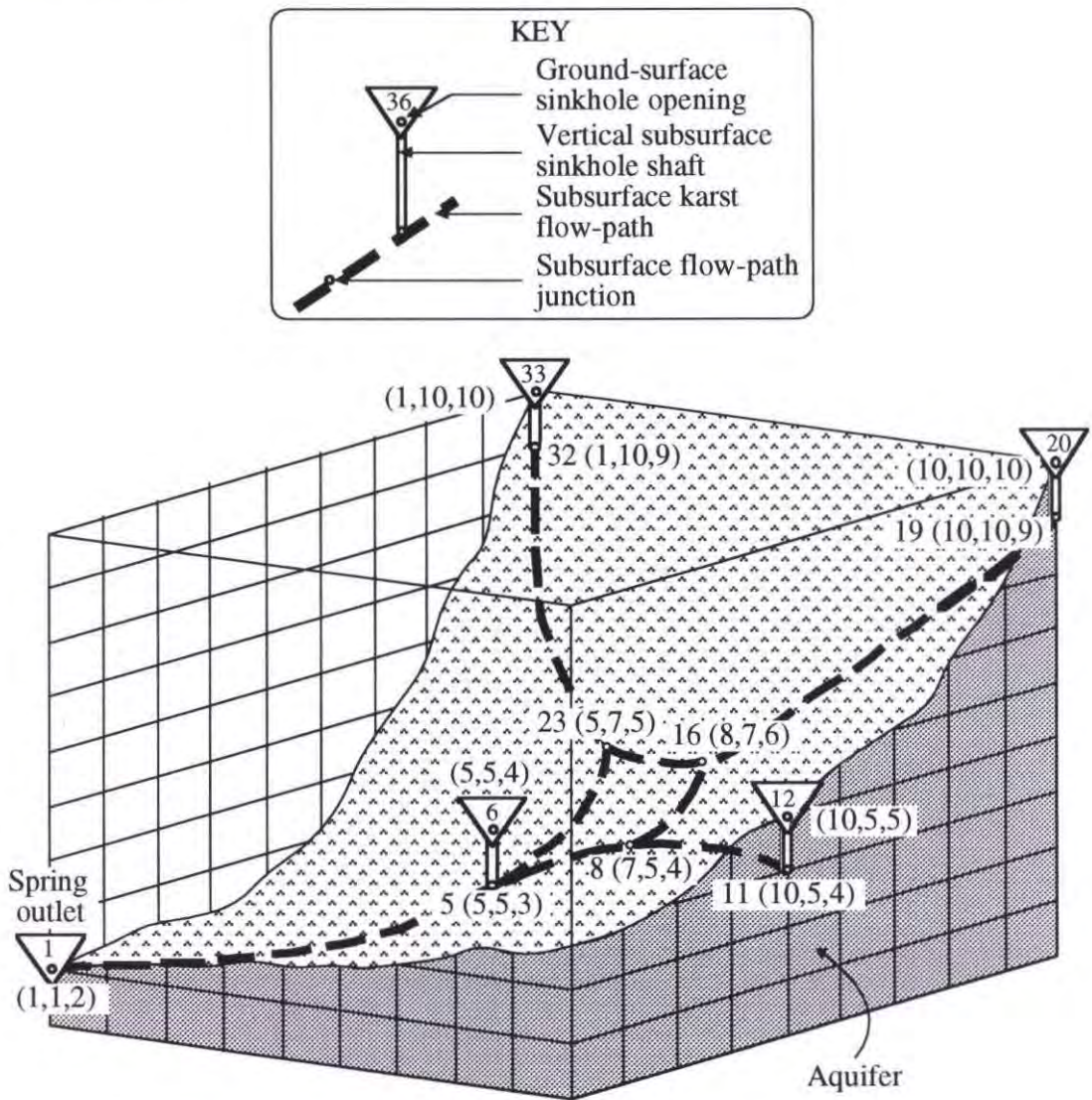


Figure 5. Schematic Representation of the Karst Aquifer

General Computational Strategy

Water and pollutant transport in the aquifer-matrix are essentially diffusive phenomena, governed by diffusion mass conservation equations whose dependent variables are heads and concentrations, respectively. Water and pollutant transport in the pipe network are essentially advective phenomena, governed by energy or momentum and mass conservation equations whose dependent variables are water discharges, heads and concentrations. The water and pollutant exchange between the aquifer-matrix and pipe network is governed essentially by the differences in head and concentration between the two systems at any node. Recall that a node is defined as an aquifer-matrix grid point through which the pipe network passes. The heads and concentrations of both systems are coupled through the water and pollutant exchange. In principle, the entire system of equations — aquifer-matrix diffusion and pipe-network energy or momentum and mass conservation — must be solved simultaneously.

This simultaneous solution poses no fundamental conceptual problems. However, its practical execution would be extremely demanding of computer resources, especially for large and/or complex systems. Therefore, a fractional-step computational strategy is adopted whereby, for each of several iterations in a computational time interval, the aquifer-matrix and pipe-network equations are solved separately, their exchange-term coupling being represented only approximately in each iteration. The details of this procedure are developed in following three main sections. The first section describes the numerical solution of the governing equation for the aquifer-matrix. The second section explains the numerical solution of the governing equation for the pipe network. The last section elaborates the numerical procedure for approximating the exchange terms between aquifer-matrix and pipe network.

Numerical Solution for Aquifer-Matrix

Strategy for Approximate Solution

The aquifer-matrix algorithm is built on the principle of water and pollutant mass conservation at aquifer-matrix elemental control volumes. Aquifer-matrix grid points are generated based on the geometry of the Big Spring aquifer (Figure 4). Figure 6 shows the schematic representation of the aquifer as adjusted to conform with the finite-difference grid. To avoid using excessive computer time and resources, the split-direction approach is used. Thus, the governing equations, at any instant, are solved successively for each direction of the principal axis in Cartesian coordinate directions within the three-dimensional block, as depicted in Figure 6.

In any computational direction, the algorithm must recognize the boundary of the domain. For example, the algorithm must recognize that there is a valley between two hills, and computations must be performed on each hill while above the valley, where there is no aquifer-matrix, computations must not be performed. The soil-topology consisting of 118 unique orientations of the aquifer-matrix grid point with respect to the origin of the Cartesian coordinate, is used to define such a geometry. One aquifer-matrix grid point associates with one unique soil-topology. Therefore, it is possible for several aquifer-matrix grid points to have the same soil-topology.

The exchange term, w (or W), is the term that actually couples the megapore network computation with that of the aquifer-matrix. The aquifer-matrix exchange inflow W^{n+1} can be written as

$$W^{n+1} = W(h_m^{n+1}, h_{ijk}^{n+1}) \quad (12)$$

that is, as some function of the pipe-network nodal head h_m^{n+1} and the aquifer-matrix head h_{ijk}^{n+1} at the aquifer-matrix grid point associated with node m , at future time t_{n+1} .

Now, in general, a Taylor-series expansion of W^{n+1} can be written as

$$W^{n+1} = W(h_m^{n+1}, h_{ijk}^{n+1}) \approx W(h_m, h_{ijk}) + \frac{\partial W}{\partial h_m} \Delta h_m + \frac{\partial W}{\partial h_{ijk}} \Delta h_{ijk} \quad (13)$$

where h_m and h_{ijk} represent the latest iterative estimates of h_m^{n+1} and h_{ijk}^{n+1} , and Δh_m and Δh_{ijk} are unknown corrections to those estimates. For convenience, Δh_{ijk} is rewritten as Δh_s so Eq. (13) becomes

$$W^{n+1} = W(h_m^{n+1}, h_s^{n+1}) \approx W(h_m, h_s) + \frac{\partial W}{\partial h_m} \Delta h_m + \frac{\partial W}{\partial h_s} \Delta h_s \quad (14)$$

Eq. (14) must be recast to conform with the split-direction approach. The source term, W^{n+1} or w^{n+1} , must be split into x -, y -, and z -directions. Thus, Eq. (14) becomes

$$\begin{aligned} W^{n+1} &= W^n + \frac{\partial W}{\partial h_s} (h^x - h^n) + \frac{\partial W}{\partial h_s} (h^y - h^x) + \frac{\partial W}{\partial h_s} (h^{n+1} - h^y) + \frac{\partial W}{\partial h_m} \Delta h_m \\ \text{or } W^{n+1} &= W^n + \frac{\partial W}{\partial h_s} (h^x - h^n) + \frac{\partial W}{\partial h_s} (h^y - h^x) + \frac{\partial W}{\partial h_s} (h^{n+1} - h^y) + \frac{\partial W}{\partial h_m} (h_m - h_m^n) \end{aligned} \quad (15)$$

where $n+1$ denotes the end of the current time step; h^n is the aquifer piezometric head at the end of the previous time step; h^x is the aquifer piezometric head at the end of the x -direction computational step; h^y is the aquifer piezometric head at the end of the y -direction computational step; h^{n+1} is the aquifer piezometric head at the end of the z -direction computational step, which is the same as the aquifer piezometric head at the end of the current time step; h_m is the latest estimate of the pipe piezometric head; and h_m^n is the pipe piezometric head at the end of the previous time step.

Now $\frac{\partial W}{\partial h_s} (h^{n+1} - h^n)$ in Eq. (11) can be rewritten as

$$\frac{\partial W}{\partial h_s} (h^{n+1} - h^y + h^y - h^x + h^x - h^n) \quad (16)$$

Substitution of Eqs. (15) and (16) into Eq. (11) yields

$$\begin{pmatrix} (1-\theta) \delta_x^2 h^n + \theta \delta_x^2 h^{n+1} - \frac{1}{3} W^n - \theta \frac{\partial W}{\partial h_s} (h^x - h^n) - \frac{\theta}{3} \frac{\partial W}{\partial h_m} (h_m - h_m^n) + \\ (1-\theta) \delta_y^2 h^n + \theta \delta_y^2 h^{n+1} - \frac{1}{3} W^n - \theta \frac{\partial W}{\partial h_s} (h^y - h^x) - \frac{\theta}{3} \frac{\partial W}{\partial h_m} (h_m - h_m^n) + \\ (1-\theta) \delta_z^2 h^n + \theta \delta_z^2 h^{n+1} - \frac{1}{3} W^n - \theta \frac{\partial W}{\partial h_s} (h^{n+1} - h^y) - \frac{\theta}{3} \frac{\partial W}{\partial h_m} (h_m - h_m^n) \end{pmatrix} = \begin{pmatrix} \frac{Sv}{\Delta t} (h^x - h^n) + \\ \frac{Sv}{\Delta t} (h^y - h^x) + \\ \frac{Sv}{\Delta t} (h^{n+1} - h^y) \end{pmatrix} \quad (17)$$

In the fractional-step sense, Eq. (17) can be generalized and written as

$$(1-\theta) \delta^2 h^n + \theta \delta^2 h^{n+1} - \frac{1}{3} W^n - \theta \frac{\partial W}{\partial h_s} (h^{n+1} - h^n) - \frac{\theta}{3} \frac{\partial W}{\partial h_m} (h_m - h_m^n) = \frac{Sv}{\Delta t} (h^{n+1} - h^n) \quad (18)$$

Discretization of Eq. (18) using the Crank-Nicholson (C-N) scheme yields

$$\begin{aligned} & (1-\theta) \{ A h_{i-1}^n - (A+B) h_i^n + B h_{i+1}^n \} + \\ & \theta \{ A h_{i-1}^{n+1} - (A+B) h_i^{n+1} + B h_{i+1}^{n+1} \} - \\ & \frac{1}{3} W^p - \theta \frac{\partial W}{\partial h_i} (h_i^{n+1} - h_i^n) - \frac{\theta}{3} \frac{\partial W}{\partial h_m} (h_m - h_m^p) = \frac{Sv}{\Delta t} (h_i^{n+1} - h_i^n) \end{aligned} \quad (19)$$

where h_m is the latest estimate of the pipe piezometric head; h_m^p is the pipe piezometric head at the end of the previous time step; A and B are known coefficients

Further manipulation and grouping the terms of Eq. (19) yields

$$\begin{aligned} -\theta A h_{i-1}^{n+1} + \left\{ \theta (A+B) + \frac{\partial W}{\partial h_i} \right\} h_i^{n+1} - \theta B h_{i+1}^{n+1} = \\ (1-\theta) \{ A h_{i-1}^n - (A+B) h_i^n + B h_{i+1}^n \} - \\ \frac{1}{3} W^p + \theta \frac{\partial W}{\partial h_i} h_i^n - \frac{\theta}{3} \frac{\partial W}{\partial h_m} (h_m - h_m^p) + \frac{Sv}{\Delta t} h_i^n \end{aligned} \quad (20)$$

for $i = 2, \dots, N-1$

In matrix form, Eq. (20) can be written as

$$[\mathbf{M}]\{\mathbf{h}\} = \{\mathbf{F}\} \quad (21)$$

where $[\mathbf{M}]$ is a tri-diagonal matrix whose $N-2$ elements comprise contributions from the

left hand side of Eq. (20), and $\{F\}$ is an $N-2$ element vector of known quantities from the right hand side of Eq. (20). In Eq. (21), there are N unknowns with $(N-2)$ equations, so two more equations from boundary conditions are needed.

Split-Direction Approach for Approximating Pollutant Transport Equations

The governing equation is recast to accommodate the split-direction approach and then the C-N scheme is applied to the equation. Equation (3) may be written, for the x-direction, as follows:

$$\Delta x \frac{\partial}{\partial x} \left(A_x D_x \frac{\partial C}{\partial x} \right) - \Delta x \frac{\partial}{\partial x} (A_x U_x C) - \frac{C_s W}{3} = v \frac{\partial C}{\partial t} \tag{22}$$

Its discretization using the Crank-Nicholson scheme yields

$$\begin{aligned} & \theta \{ A C_{i-1}^{n+1} - (A+B) C_i^{n+1} + B C_{i+1}^{n+1} \} + \\ & (1-\theta) \{ A C_{i-1}^n - (A+B) C_i^n + B C_{i+1}^n \} - \\ & \frac{\theta}{2} (A_r C_{i+1}^{n+1} U_{i+1}^{n+1} + (A_r - A_l) C_i^{n+1} U_i^{n+1} - A_l C_{i-1}^{n+1} U_{i-1}^{n+1}) - \\ & \frac{(1-\theta)}{2} (A_r C_{i+1}^n U_{i+1}^n + (A_r - A_l) C_i^n U_i^n - A_l C_{i-1}^n U_{i-1}^n) - \\ & \theta \frac{C_s^{n+1} W_i^{n+1}}{3} - (1-\theta) \frac{C_s^n W_i^n}{3} = \frac{v (C_i^{n+1} - C_i^n)}{\Delta t} \end{aligned} \tag{23}$$

for $i = 2, \dots, N-1$

where A_r and A_l indicate the area of the right and left sides of a finite-difference block.

Eq. (23) can be written, in matrix form, as

$$[M]\{C\} = \{F\} \tag{24}$$

where $[M]$ is a tri-diagonal matrix whose $N-2$ elements comprise contributions from the left hand side of Eq. (23); $\{F\}$ is an $N-2$ element vector of known quantities from the right hand side of Eq. (23); and $\{C\}$ is an $N-2$ element vector of unknown pollutant concentrations.

Numerical Solution for Megapores

The numerical solution for megapores is achieved by first solving the hydrodynamic equations and then the pollutant transport equation. For hydrodynamic equations, the so-called Preissmann method is used. For pollutant transport, the split-process approach is used. First, the pure advection equation is solved by a characteristic method using the Holly-Preissmann technique. Second, the pure diffusion equation is solved by the Preissmann method. The advantage of solving the pollutant transport equation using the split-process approach is that one can then compute any complex network in a downstream-marching fashion. That is, the computation starts from the most upstream point in the network and proceeds until it reaches the most downstream node. The split approach saves computer time since it avoids inverting a large matrix as is done in a direct approach.

Approximate Solution of Hydrodynamic Equations

Strategy for Approximate Solution

The megapore network, on which all megapore computations are carried out in the study, is manually generated based on data obtained from the study done by Hallberg et al. (1983). The gross megapore layout is presumed to follow gross flow paths from field data. The two-dimensional representation of the network is given in Figure 7. All horizontal, almost horizontal, and vertical megapores are represented in Figure 7.

The megapore network algorithm is built on the principle of water mass conservation at looped nodes. A looped node is defined herein as a node (i.e., aquifer-matrix grid point through which the pipe network passes) which is either

1. an entrance to or exit from the network, or
2. a junction of multiple (more than two) flow paths.

Thus, by this definition, nodes 1, 5, 6, 8, 12, 16, 20, 23, and 33 in Figure 5 are all looped nodes. Any unique flow path linking two looped nodes is defined herein as a link. In connecting two looped nodes, a link may pass through other nodes which are not looped; these are called inline nodes. Any two adjacent nodes, be they inline or looped, are connected by a segment of a link called a pipe. A link may comprise only one pipe. Finally, any pipe can be divided into a series of computational points connected by computational reaches. A pipe always has one computational point contiguous with the node to which it is attached at each end. Figures 8 and 9 summarize these definitions.

Nodal Continuity

At any node m , and in particular at any looped node, the following statement of water continuity (inflow = outflow) must be satisfied at any instant (see Figure 10):

$$\sum_{lp} Q_{lp}^{n+1} + Q_m^{n+1} + W_m^{n+1} = 0, \quad m = 1, 2, 3, \dots \quad (25)$$

where $n+1$ denotes the end of the current time step; Q_{lp}^{n+1} is discharge entering node m from pipe lp ; Q_m^{n+1} is external inflow entering node m ; W_m^{n+1} is inflow entering node m from the aquifer-matrix; and summation is over all the pipes attached to node m (one at the end of each attached link).

Now, the external inflow Q_m^{n+1} is a known quantity; indeed at boundary nodes, it is the sinkhole or other point inflow which drives the system. The pipe inflow can be written as

$$Q_{lp}^{n+1} = Q_p + \Delta Q_{lp} \quad (26)$$

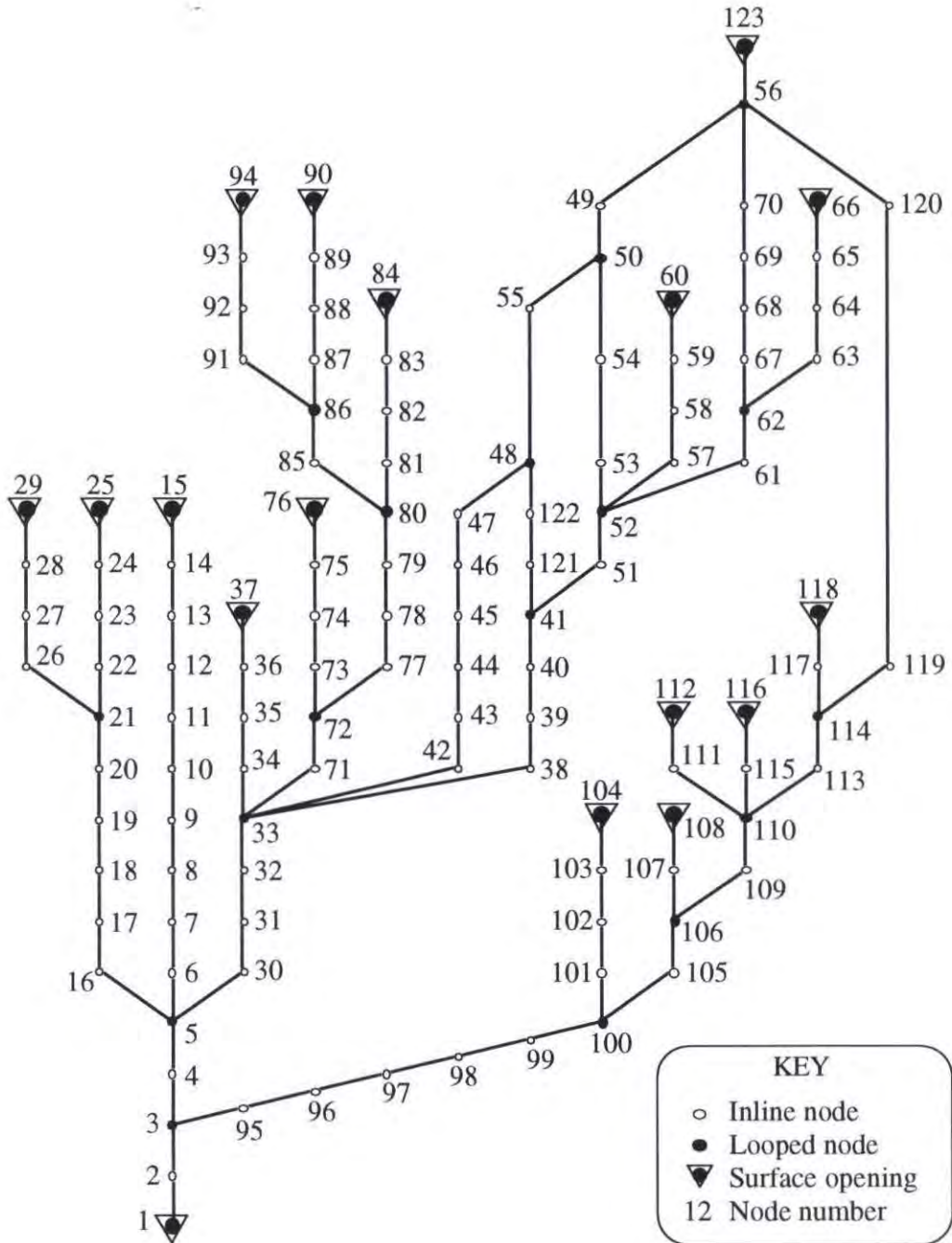


Figure 7. Schematic Representation of the Megapore Network

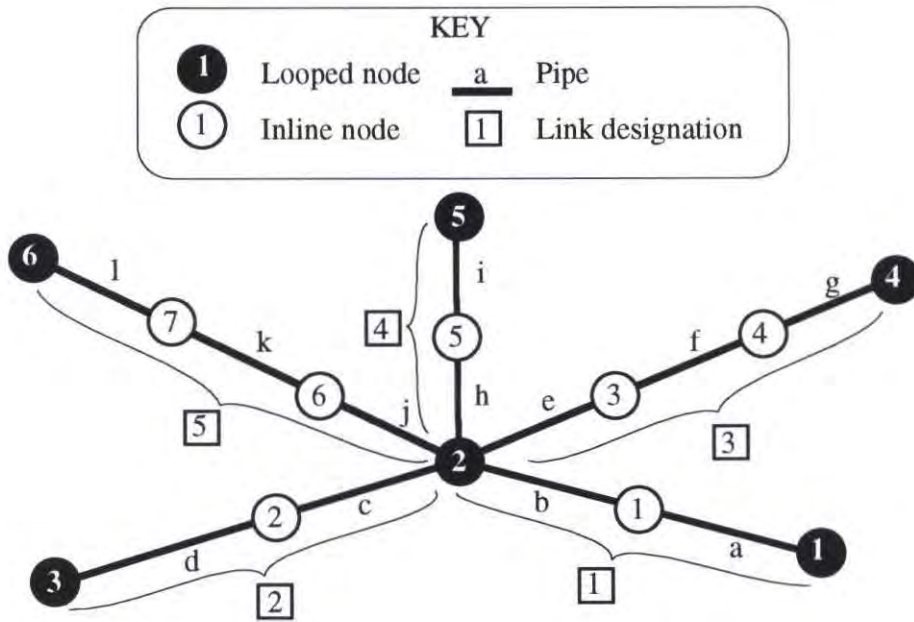


Figure 8. Megapore Topological Definitions

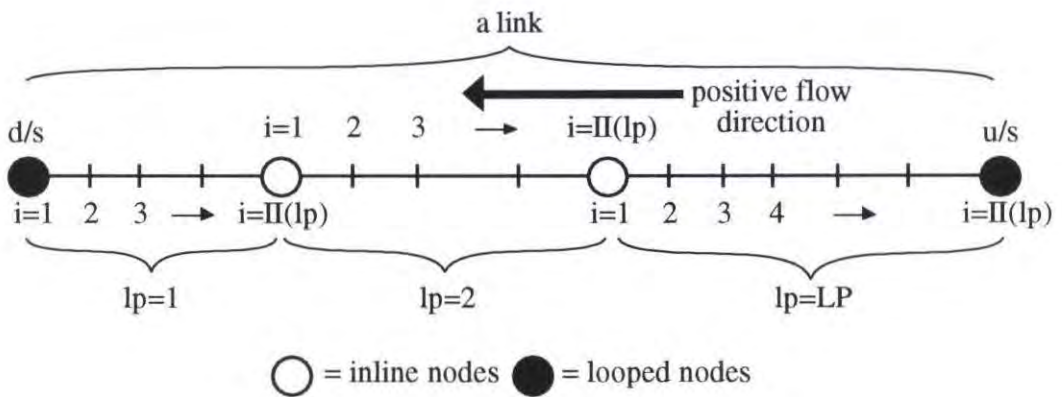


Figure 9. Definition Sketch for Link/Pipe Computation

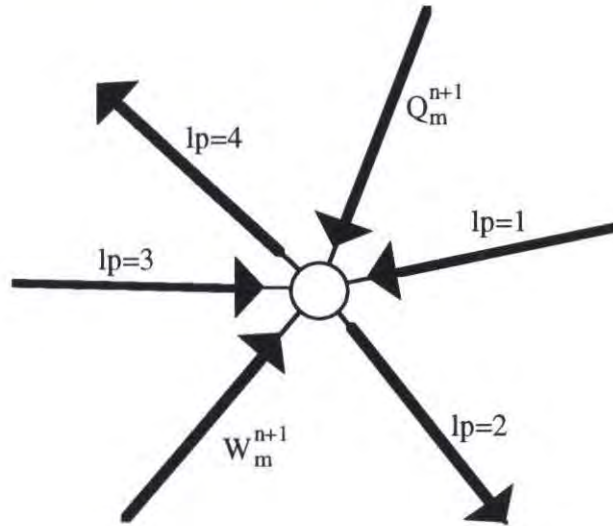


Figure 10. Continuity at a Looped Node

where Q_p is the latest iterative estimate of Q_p^{n+1} , and ΔQ_p is an unknown correction to that estimate.

The aquifer-matrix exchange inflow W_m^{n+1} can be written as

$$W_m^{n+1} = W (h_m^{n+1}, h_{ijk}^{n+1}) \tag{27}$$

That is, the aquifer-matrix exchange inflow is represented as a function of the pipe-network nodal head h_m^{n+1} and the aquifer-matrix head h_{ijk}^{n+1} at the aquifer-matrix grid point associated with node m . The Taylor-series expansion of W_m^{n+1} is

$$W_m^{n+1} = W (h_m^{n+1}, h_{ijk}^{n+1}) \approx W (h_m, h_{ijk}) + \frac{\partial W}{\partial h_m} \Delta h_m + \frac{\partial W}{\partial h_{ijk}} \Delta h_{ijk} \tag{28}$$

where h_m and h_{ijk} represent the latest iterative estimates of h_m^{n+1} and h_{ijk}^{n+1} , and Δh_m and Δh_{ijk} are unknown corrections to those estimates.

In fractional-step computations, the aquifer-matrix heads h_{ijk}^{n+1} are held fixed during the pipe-network computation. Consequently, in Eq. (28), $\Delta h_{ijk} = 0$, and substitution of Eqs. (26) and (28) into Eq. (25) yields

$$\sum_{lp} (Q_{lp} + \Delta Q_{lp}) + Q_m^{n+1} + W_m + \frac{\partial W}{\partial h_m} \Delta h_m = 0, \quad m = 1, 2, \dots \tag{29}$$

$$\text{or } \sum_{in} (Q_d + \Delta Q_d) - \sum_{out} (Q_u + \Delta Q_u) + Q_m^{n+1} + W_m + \frac{\partial W}{\partial h_m} \Delta h_m = 0, \quad m = 1, 2, \dots \tag{30}$$

Equation (30) is not yet in a form which can be used to compute head corrections, since Δh_m , as well as two or more ΔQ_{lp} , are unknowns. The key to the solution algorithm is the manipulation of the finite-difference approximations for the pipe-flow equations. These can be made to yield linear relations between discharge corrections ΔQ_{lp} and nodal head corrections Δh_{mm} at looped nodes mm at either end of a link. In particular, for a link whose upstream node is denoted u and whose downstream node is denoted d , we can derive the following two relations:

$$\Delta Q_d = \frac{\Delta h_u - FF_u - HH_u \Delta h_d}{EE_u} \quad (31)$$

$$\Delta Q_u = \frac{\Delta h_u - F_u - H_u \Delta h_d}{E_u} \quad (32)$$

where ΔQ_d and ΔQ_u are the discharge corrections at the pipe computational points contiguous with nodes d and u ; Δh_d and Δh_u are the head corrections at nodes d and u ; and E_u , F_u , H_u , EE_u , FF_u , and HH_u are known coefficients derived in the link forward sweep as described below.

In Eq. (30), the summation over the pipes connected to a node can be thought of as a summation over the connected links, as each connected pipe is simply the end of a link. Moreover, the summation implies consistent recognition of pipe sign conventions, with inflows taken as positive and outflows taken as negative. Substitution of Eqs. (31) and (32) into Eq. (30) yields

$$\sum_{in} Q_d + \sum_{in} \frac{\Delta h_u - FF_u - HH_u \Delta h_m}{EE_u} - \sum_{out} Q_u - \sum_{out} \frac{\Delta h_m - F_u - H_u \Delta h_d}{E_u} + Q_m^{n+1} + W_m + \frac{\partial W}{\partial h_m} \Delta h_m = 0 \quad (33)$$

As seen in Figure 11, in the "in" summation, Δh_d represents the current node Δh_m , and Δh_u represents the looped node at the other end of the inflow link. Similarly, in the "out" summation, Δh_u represents the current node Δh_m , and Δh_d represents the looped node at the other end of the outflow link. Therefore, Eq. (33) can be rewritten as

$$\left(\frac{\partial W}{\partial h_m} - \sum_{in} \frac{HH_u}{EE_u} - \sum_{out} \frac{1}{E_u} \right) \Delta h_m + \sum_{in} \frac{1}{EE_u} \Delta h_u + \sum_{out} \frac{H_u}{E_u} \Delta h_d = - \sum_{in} \left(Q_d - \frac{FF_u}{EE_u} \right) + \sum_{out} \left(Q_u - \frac{F_u}{E_u} \right) - Q_m^{n+1} - W_m \quad \text{for } m = 1, 2, \dots \quad (34)$$

Since Eq. (34) can be written for each of M looped nodes, the entire system of linear equations is:

$$[\mathbf{A}]\{\Delta \mathbf{h}_m\} = \{\mathbf{B}\} \quad (35)$$

where $[\mathbf{A}]$ is an $M \times M$ coefficient matrix whose elements comprise contributions from the left hand side of Eq. (34); $\{\mathbf{B}\}$ is an M -element vector of known quantities from the right

hand side of Eq. (34); and $\{\Delta h_m\}$ is the M-element vector of unknown corrections to heads at looped nodes.

Solving Eq. (34) yields the head corrections $\{\Delta h_m\}$. Thus the looped nodal heads can be corrected immediately.

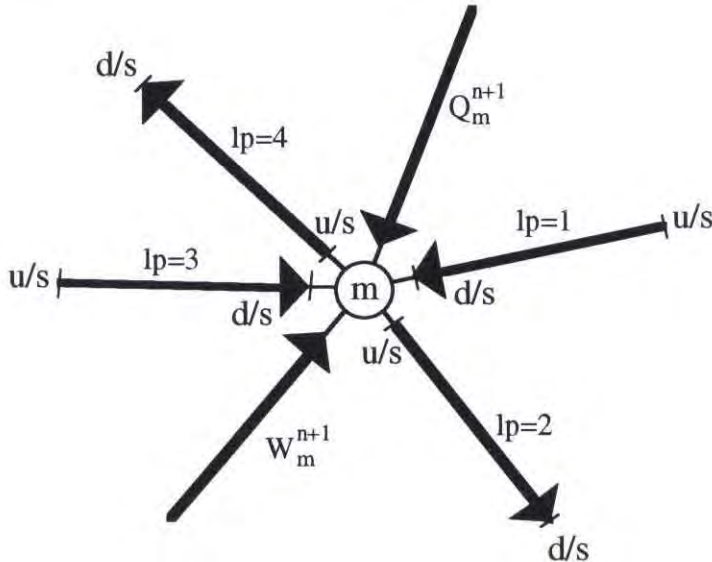


Figure 11. Summation Definition at a Node

Pipe Flow Dynamics

The coefficients of Eqs. (31) and (32), result from a so-called *forward sweep* in which the appropriate pipe conservation equations are expressed algebraically through use of finite-difference approximations.

Using Preissmann’s four-point scheme (Cunge et al., 1980) to discretize Eq. (6) for a reach between two computational points i and $i+1$ (see Figure 9) yields

$$\begin{aligned} & \frac{Q^{n+1} - Q^n}{\Delta t} - \left[\varphi \left(\frac{(Q/A)_i^{n+1} + (Q/A)_{i+1}^{n+1}}{2} \right)^2 + (1-\varphi) \left(\frac{(Q/A)_i^n + (Q/A)_{i+1}^n}{2} \right)^2 \right] \times \\ & \left[\varphi \frac{A_i^{n+1} - A_{i+1}^{n+1}}{\Delta s} + (1-\varphi) \frac{A_i^n - A_{i+1}^n}{\Delta s} \right] + \\ & g \left(\varphi \frac{A_i^{n+1} + A_{i+1}^{n+1}}{2} + (1-\varphi) \frac{A_i^n + A_{i+1}^n}{2} \right) \left\{ \varphi \frac{h_i^{n+1} - h_{i+1}^{n+1}}{\Delta s} + (1-\varphi) \frac{h_i^n - h_{i+1}^n}{\Delta s} + \right. \\ & \left. \frac{\varphi}{2} \left(\frac{Q^{n+1} |Q^{n+1}|}{K_i^2} + \frac{Q^{n+1} |Q^{n+1}|}{K_{i+1}^2} \right) + \frac{1-\varphi}{2} \left(\frac{Q^n |Q^n|}{K_i^2} + \frac{Q^n |Q^n|}{K_{i+1}^2} \right) \right\} = 0 \end{aligned} \tag{36}$$

where the n and $n+1$ superscripts denote times t_n and $t_{n+1} = t_n + \Delta t$; Δs denotes the length of

the computational reach; and ϕ is Preissmann’s time weighting parameter, $0.5 \leq \phi \leq 1.0$. It should be noted that the full-pipe invariance of Q along the pipe obviates the need for a computational point subscript on Q .

In Eq. (36), all quantities with $n+1$ superscripts are unknown. Since the pipe area and conveyance are known quantities for the full-pipe situation, Eq. (36) can be written as

$$F(Q^{n+1}, h_i^{n+1}, h_{i+1}^{n+1}) = 0 \tag{37}$$

As long as the function F is continuous in the neighborhood of the solution, Eq. (37) can be written as the first term of the Taylor-series expansion

$$F(Q^{n+1}, h_i^{n+1}, h_{i+1}^{n+1}) \approx F(Q, h_i, h_{i+1}) + \frac{\partial F}{\partial Q} \Delta Q + \frac{\partial F}{\partial h_i} \Delta h_i + \frac{\partial F}{\partial h_{i+1}} \Delta h_{i+1} \tag{38}$$

in which $Q, h_i,$ and h_{i+1} are the latest available estimate of $Q^{n+1}, h_i^{n+1},$ and h_{i+1}^{n+1} . It is understood that the partial derivatives $\frac{\partial F}{\partial Q}, \frac{\partial F}{\partial h_i},$ and $\frac{\partial F}{\partial h_{i+1}}$ are evaluated at (Q^n, h_i^n, h_{i+1}^n) .

Symbolically, Eq. (38) can be written as

$$a_i \Delta Q_{lp} + b_i \Delta h_{i,lp} + c_i \Delta h_{i+1,lp} + d_i = 0 \tag{39}$$

where $a_i = \frac{\partial F}{\partial Q}, b_i = \frac{\partial F}{\partial h_i}, c_i = \frac{\partial F}{\partial h_{i+1}},$ and $d_i = F(Q, h_i, h_{i+1})$ (40)

Armed with Eq. (39), one can now proceed with the derivations leading to Eqs. (31) and (32) for each link. The general idea is to conduct a forward sweep from the first (downstream) computational point of the first (downstream) pipe of a link, through successive inline nodes and pipes, to arrive at the last (upstream) pipe of the link. The “u” subscript of Eqs. (31) and (32) refers to this last point at the end of the forward sweep along a link. For the forward sweep derivations, it is useful to use a double subscript (i,lp) to designate point i on pipe lp; LP denotes the last pipe on the link, and II(lp) denotes the last point on pipe lp.

After a forward sweep for a link ends at the last point II(LP) of the last pipe LP, one may deduce the following relation

$$\Delta h_{II(LP),LP} = E_{II(LP),LP} \Delta Q_{LP} + F_{II(LP),LP} + H_{II(LP),LP} \Delta h_{1,1} \tag{41}$$

Eq. (41) is essentially equivalent to Eq. (32) with “u” denoting the last point of the link (II(LP),LP) and “d” denoting the first point (1,1). From a similar derivation, one may deduce the following relation as well:

$$\Delta h_{II(LP),LP} = EE_{II(LP),LP} \Delta Q_1 + FF_{II(LP),LP} + HH_{II(LP),LP} \Delta h_{1,1} \tag{42}$$

It should be noted that this equation is the same as Eq.(31), where “u” denotes the last point of the link and “d” denotes the first one, as in Eq. (32).

All the influence coefficients of Eqs. (41) and (42), that is E, F, H, EE, FF, and HH, are computed during the forward sweep. Thus, head corrections for all looped nodes can be computed using Eq. (35). A “backward sweep,” in which the discharge correction and the head correction for all computational points in each pipe are computed, can now be performed for each link. At the end of a complete sweep, piezometric head and discharge of all pipes in a network are updated. One can thus proceed to the next time step computation.

Approximate Solution for Pollutant Transport Equations

Strategy for Approximate Solution

Sauvaget (1982) points out that Eq. (7) represents two physical phenomena; i.e., advection and diffusion. The mathematical nature of the advection equation, Eq. (43), and the diffusion equation, Eq. (58), in which the diffusion equation poses fewer numerical problems than the advection one, justifies the adoption of different solution methods. Thus, the solution of Eq. (7) is split into two processes for each time step; Eqs. (43) and (58) are solved successively by computational schemes that are appropriate to each of them.

Usseglio-Polatera and Chenin-Mordojovich (1988) show that process-splitting is particularly attractive for 2-D and 3-D simulations in water resources. Within each elementary fractional step, the cost of using stable implicit procedures or specially adapted schemes is small, especially when space-splitting is combined with process-splitting. This combination leads to accurate, powerful and cost-effective schemes with no formal limitations. Furthermore, this splitting framework makes possible a combination of competing numerical techniques (characteristics, finite-differences, finite elements) when these techniques are complementary.

The extension of process-splitting to a megapore network is straightforward; the approach permits calculation of pollutant concentration by proceeding from the most upstream to the most downstream point in the network. This is done by (1) ordering all computational points from upstream to downstream and, (2) applying the process-splitting technique at each megapore and mass conservation law at each node. Since the approach avoids inverting a large matrix, overall computer time used in the computations decreases.

Advection Computation

The advective process is described by the following equation:

$$A \frac{\partial C}{\partial t} + AU \frac{\partial C}{\partial x} = 0 \quad \text{or} \quad \frac{\partial C}{\partial t} + U \frac{\partial C}{\partial x} = 0 \quad (43)$$

Since the velocity U is independent of the concentration C , one may write $U = \frac{dx}{dt}$ and rewrite Eq. (43) as

$$\frac{\partial C}{\partial t} + \frac{dx}{dt} \frac{\partial C}{\partial x} = 0 \quad \text{or} \quad \frac{dC}{dt} = 0 \tag{44}$$

This means that the value of C attached to a fluid volume remains constant during the movement along its characteristic line. Now the integration of Eq. (44) along this line as depicted in Figure 12 yields

$$C_i^{n+1} = C_\xi^n \tag{45}$$

where C_i^{n+1} is the pollutant concentration at node i at the current time step, and C_ξ^n is the pollutant concentration at the foot of the characteristic line at the previous time step. The term C_ξ^n in the right hand side of Eq. (45), is estimated using the Holly-Preissmann third-degree interpolating polynomial as described in the following paragraphs (see Holly et al., 1977). Estimating C_ξ^n using the concentration C and gradient concentration CX from the two neighboring points of x by constructing the third-order polynomial gives

$$C_\xi^n \approx y(\alpha) = A\alpha^3 + B\alpha^2 + D\alpha + E \tag{46}$$

in which

$$\alpha = \frac{x_{i-k} - x}{\Delta x} = \frac{U\Delta t - k\Delta x}{\Delta x} = Cr - k \tag{47}$$

and

$$Cr = \frac{U\Delta t}{\Delta x} \tag{48}$$

is the Courant number and k is the integer part of Cr.

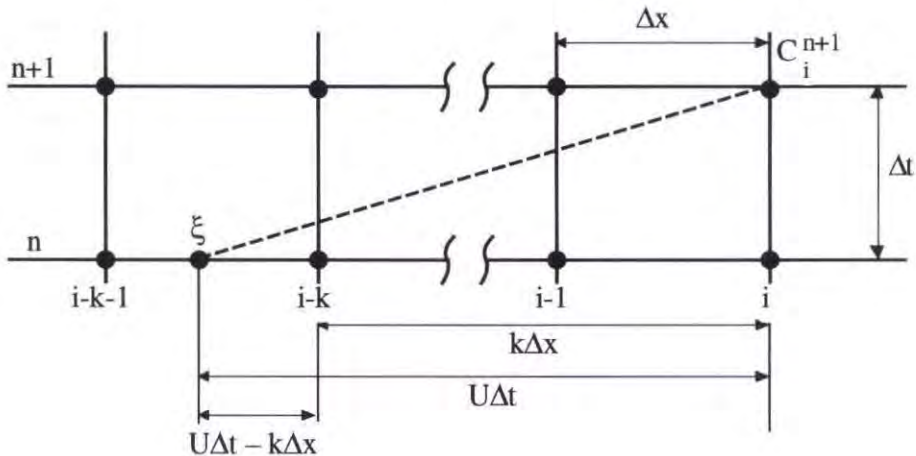


Figure 12. Characteristic Curve on Advection Grid System

The four coefficients A, B, D, and E can be evaluated such that the following four conditions are satisfied:

$$y(0) = C_{i-k}^n; y(1) = C_{i-k-1}^n; \left. \frac{dy}{dx} \right|_{\alpha=0} = CX_{i-k}^n; \left. \frac{dy}{dx} \right|_{\alpha=1} = CX_{i-k-1}^n \tag{49}$$

Through the chain rule of differentiation, $\frac{dy}{dx} = \frac{dy}{d\alpha} \frac{d\alpha}{dx} = \frac{dy}{d\alpha} \frac{-1}{\Delta x}$ which is applied to Eq. (46), the four coefficients A, B, D, and E can be computed as

$$\left. \begin{aligned} A &= -2 C_{i-k-1}^n + 2 C_{i-k}^n - \Delta x CX_{i-k-1}^n - \Delta x CX_{i-k}^n \\ B &= 3 C_{i-k-1}^n - 3 C_{i-k}^n + \Delta x CX_{i-k-1}^n + 2 \Delta x CX_{i-k}^n \\ D &= -\Delta x CX_{i-k}^n \\ E &= C_{i-k}^n \end{aligned} \right\} \tag{50}$$

Substitution of Eq. (50) into Eq. (46) yields

$$C_{\xi}^n = a_1 C_{i-k-1}^n + a_2 C_{i-k}^n + a_3 CX_{i-k-1}^n + a_4 CX_{i-k}^n \tag{51}$$

in which

$$\left. \begin{aligned} a_1 &= \alpha^2 (3 - 2 \alpha) \\ a_2 &= 1 - a_1 \\ a_3 &= \alpha^2 (1 - \alpha) \Delta x \\ a_4 &= -\alpha (1 - \alpha)^2 \Delta x \end{aligned} \right\} \tag{52}$$

where

$$\Delta x = x_{i-k} - x_{i-k-1}$$

One can also evaluate CX_{ξ}^n from Eq. (51) as

$$CX_{\xi}^n = \frac{\partial C}{\partial x} = b_1 C_{i-k-1}^n + b_2 C_{i-k}^n + b_3 CX_{i-k-1}^n + b_4 CX_{i-k}^n \tag{53}$$

in which

$$\left. \begin{aligned} b_1 &= \frac{6 \alpha (\alpha - 1)}{\Delta x} \\ b_2 &= -b_1 \\ b_3 &= \alpha (3 \alpha - 2) \\ b_4 &= (\alpha - 1) (3 \alpha - 1) \end{aligned} \right\} \tag{54}$$

From Eq. (51) it is obvious that to solve the problem completely one has to keep track of not only the concentration C_i^n but also CX_i^n for the next time step. This can be done by taking the derivative of Eq. (43) with respect to x:

$$\frac{\partial}{\partial x} \left(\frac{\partial C}{\partial t} \right) + U \frac{\partial}{\partial x} \left(\frac{\partial C}{\partial x} \right) = - \frac{\partial C}{\partial x} \frac{\partial U}{\partial x}$$

or

$$\frac{\partial}{\partial t}(CX) + U \frac{\partial}{\partial x}(CX) = -CX \frac{\partial U}{\partial x}$$

or

$$\frac{d(CX)}{dt} = -CX \frac{\partial U}{\partial x} \tag{55}$$

For the gradient concentration CX, one may write the direct analogy of Eqs. (44) and (45) using the technique used to compute concentration C:

$$CX_i^{n+1} = CX_\xi^n - \int_{t_n}^{t_{n+1}} CX \frac{\partial U}{\partial x} dt \tag{56}$$

This is approximated as

$$CX_i^{n+1} = CX_\xi^n - \frac{\Delta t}{2} \left[CX_\xi^n \left[\frac{\partial U}{\partial x} \right]_\xi + CX_i^{n+1} \left[\frac{\partial U}{\partial x} \right]_i \right]$$

Solving for CX_i^{n+1} , one obtains

$$CX_i^{n+1} = CX_\xi^n \left[\frac{1 - \frac{\Delta t}{2} \left[\frac{\partial U}{\partial x} \right]_\xi}{1 + \frac{\Delta t}{2} \left[\frac{\partial U}{\partial x} \right]_i} \right] \tag{57}$$

where CX_ξ^n can be evaluated using Eq. (53)

Diffusion Computation

The diffusive process is described by the following equation:

$$A \frac{\partial C}{\partial t} = \frac{\partial}{\partial x} (A \epsilon_x \frac{\partial C}{\partial x}) \tag{58}$$

Eq. (58) is a second-order partial differential equation that can be transformed into an equivalent system of two equations of the first order:

$$\begin{aligned} A \frac{\partial C}{\partial t} &= \frac{\partial}{\partial x} (A \epsilon_x CX) \\ \frac{\partial C}{\partial x} &= CX \end{aligned} \tag{59}$$

in which concentration C and its gradient CX are the dependent variables. Using the following notation such that

$$\begin{aligned}\Delta x &= x_i - x_{i-1} \\ \Delta C_i &= C_i^{n+1} - C_i^n \\ \Delta CX_i &= CX_i^{n+1} - CX_i^n\end{aligned}\tag{60}$$

and a discretization scheme devised by A. Preissmann, which adopts the approximations,

$$\begin{aligned}f(x,t) &= \frac{\theta}{2}(f_i^{n+1} + f_{i-1}^{n+1}) + \frac{1-\theta}{2}(f_i^n + f_{i-1}^n) \\ &= \frac{\theta}{2}(\Delta f_i + \Delta f_{i-1}) + \frac{1}{2}(f_i^n + f_{i-1}^n) \\ \frac{\partial f}{\partial x} &= \theta \frac{f_i^{n+1} - f_{i-1}^{n+1}}{\Delta x} + (1-\theta) \frac{f_i^n - f_{i-1}^n}{\Delta x} \\ &= \frac{\theta}{\Delta x}(\Delta f_i - \Delta f_{i-1}) + \frac{1}{\Delta x}(f_i^n - f_{i-1}^n) \\ \frac{\partial f}{\partial t} &= \frac{(f_i^{n+1} - f_i^n) + (f_{i-1}^{n+1} - f_{i-1}^n)}{2\Delta t} \\ &= \frac{1}{2\Delta t}(\Delta f_i + \Delta f_{i-1})\end{aligned}$$

Eq. (59) becomes the discretized system:

$$\begin{aligned}\frac{\theta}{\Delta x}(\Delta C_i - \Delta C_{i-1}) + \frac{1}{\Delta x}(C_i^n - C_{i-1}^n) &= \frac{\theta}{2}(\Delta CX_i + \Delta CX_{i-1}) + \frac{1}{2}(CX_i^n + CX_{i-1}^n) \\ \frac{A}{2\Delta t}(\Delta C_i + \Delta C_{i-1}) &= A \varepsilon_x \left(\frac{\theta}{\Delta x}(\Delta CX_i - \Delta CX_{i-1}) + \frac{1}{\Delta x}(CX_i^n - CX_{i-1}^n) \right) + \\ &\quad \frac{\partial A}{\partial x} \varepsilon_x \left(\frac{\theta}{2}(\Delta CX_i + \Delta CX_{i-1}) + \frac{1}{2}(CX_i^n + CX_{i-1}^n) \right)\end{aligned}$$

This system can be rewritten as

$$\left. \begin{aligned}a_1 \Delta C_i + a_2 \Delta CX_i + a_3 \Delta C_{i-1} + a_4 \Delta CX_{i-1} + a_5 &= 0 \\ b_1 \Delta C_i + b_2 \Delta CX_i + b_3 \Delta C_{i-1} + b_4 \Delta CX_{i-1} + b_5 &= 0\end{aligned} \right\} \text{for } i = 2, 3, \dots, N\tag{61}$$

where

$$\begin{aligned}a_1 &= \frac{\theta}{\Delta x} \\ a_2 &= -\frac{\theta}{2} \\ a_3 &= -a_1 \\ a_4 &= a_2 \\ a_5 &= \frac{C_i^n - C_{i-1}^n}{\Delta x} - \frac{CX_i^n + CX_{i-1}^n}{2}\end{aligned}$$

$$\begin{aligned}
 b_1 &= -\frac{A}{2\Delta t} \\
 b_2 &= \theta \varepsilon_x \left(0.5 \frac{\partial A}{\partial x} + \frac{A}{\Delta x}\right) \\
 b_3 &= b_1 \\
 b_4 &= \theta \varepsilon_x \left(0.5 \frac{\partial A}{\partial x} - \frac{A}{\Delta x}\right) \\
 b_5 &= \varepsilon_x \frac{\partial A}{\partial x} \frac{CX_i^n + CX_{i-1}^n}{2} + \varepsilon_x A \frac{CX_i^n - CX_{i-1}^n}{\Delta x}
 \end{aligned}$$

Eq. (61) may be solved efficiently using the classic double-sweep algorithm.

Elimination of ΔCX_{i-1} from Eq. (61) yields

$$\Delta C_{i-1} = L_{i-1} \Delta C_i + M_{i-1} \Delta CX_i + N_{i-1} \tag{62}$$

where

$$L_{i-1} = \frac{a_1 b_4 - a_4 b_1}{a_4 b_3 - a_3 b_4}, \quad M_{i-1} = \frac{a_2 b_4 - a_4 b_2}{a_4 b_3 - a_3 b_4}, \quad \text{and} \quad N_{i-1} = \frac{a_5 b_4 - a_4 b_5}{a_4 b_3 - a_3 b_4} \tag{63}$$

To obtain a relationship that is useful for computing the influence coefficients of the double-sweep method, let $\Delta CX_{i-1} = Q_{i-1} \Delta C_{i-1} + R_{i-1}$. Substituting this relationship and Eq. (62) into Eq. (61), and solving for ΔCX_i , yields

$$\Delta CX_i = Q_i \Delta C_i + R_i \tag{64}$$

where

$$S_i = a_3 + a_4 Q_{i-1}, \quad Q_i = -\frac{a_1 + L_{i-1} S_i}{a_2 + M_{i-1} S_i}, \quad R_i = -\frac{a_5 + N_{i-1} S_i + a_4 R_{i-1}}{a_2 + M_{i-1} S_i} \tag{65}$$

One can solve the system of Eq. (61) recursively, using Eqs. (62) and (64), given the appropriate boundary conditions.

Iterative Coupling of Megapore and Aquifer-Matrix Computation

As previously mentioned, a fractional-step method is used to approximate the governing equations. In each time step during the simulation, the computations in the megapore network and those in the aquifer-matrix are coupled through the source or exchange term of the governing equation. For clarity, Eqs. (15) are repeated below.

$$W^{n+1} = W^n + \frac{\partial W}{\partial h_s} (h^x - h^n) + \frac{\partial W}{\partial h_s} (h^y - h^x) + \frac{\partial W}{\partial h_s} (h^{n+1} - h^y) + \frac{\partial W}{\partial h_m} (h_m - h_m^n) \tag{15}$$

$$\sum_{lp} Q_{lp}^{n+1} C_{lp}^{n+1} + Q_m^{n+1} C_m^{n+1} + W_m^{n+1} C_s = 0, \quad m = 1, 2, 3, \dots \tag{66}$$

where n+1 denotes the end of the current time step; h_m is the latest estimate of the pipe

piezometric head; W_m^{n+1} is inflow entering node m from the aquifer-matrix; C_s is the latest estimate of pollutant concentration of node m from the aquifer, and all other symbols are as previously defined.

In each time step, the last terms in Eqs. (15) and (66) represent the latest estimate of exchange mass between the megapore network and aquifer-matrix. The fractional-step computations have to be carried out until this estimate converges according to some criterion. Thus the fractional step of the hydrodynamic computation will stop when the latest estimate of the megapore piezometric head h_m in Eq. (15) satisfies a certain convergence criterion, after which the pollutant computations begin. As with the hydrodynamic computation, the fractional step of the pollutant transport computation will stop after the latest estimates of pollutant fluxes ($W_m^{n+1} C_s$) in Eq. (66) satisfy a certain convergence criterion. Thus, in each time step, the fractional-step computations are iterated until the convergence criterion is satisfied.

TEST AND APPLICATION

This chapter presents tests and applications of the model to the Big Spring Basin. Sensitivity analyses of important system parameters of this basin (megapore diameter, roughness coefficient, hydraulic conductivity of the aquifer, and classes of megapore diameter) are conducted to identify interaction between the parameters and model components. Simulation of dye trace experiments conducted in the basin is performed to demonstrate the capability of the model.

Water Quality Responses of the Big Spring Basin

If the present model is to serve as the basis for a broader range of research, it must be shown to be able to simulate field conditions. To do this, the model was run to simulate two of the dye trace experiments conducted by Hallberg et al. (1983). The purpose of these experiments was to establish direct connections between sinkhole recharge points and discharging springs. In the Big Spring Basin, several dye trace experiments were conducted by the Iowa Conservation Commission (ICC) and Iowa Geological Survey (IGS). Figure 13 shows the sinkholes used as dye input points (Hallberg et al. 1983).

Simulation of Dye Trace Experiments

In the dye trace experiments, Fluorescein dye was placed at the sinkholes. At least one week prior to both traces, packets of activated coconut charcoal were placed at the collection points. This coconut charcoal was used to capture Fluorescein from the water. These were replaced with fresh packets the day before each trace and tested for background levels of Fluorescein which, if present, could result in a false trace. Background levels at all collection points tested negative (Hallberg et al., 1983). In the present simulation, Big Spring is the only collection point considered.

The first dye trace experiment simulated here is the one conducted on the Bugenhagen farm (trace A, see Figure 13). The experiment began at 8:30 pm, when 2 pounds of Fluorescein dye were placed in a sinkhole on the farm. At that time, a stream flow of 0.02–0.05 cfs was draining directly into the sinkhole. Charcoal packets were changed periodically at Big Spring, with the first dye appearing between 39 and 51 hours after the input. Flow at Big Spring during this period varied from 62 to 65 cfs (Hallberg et al.

1983).

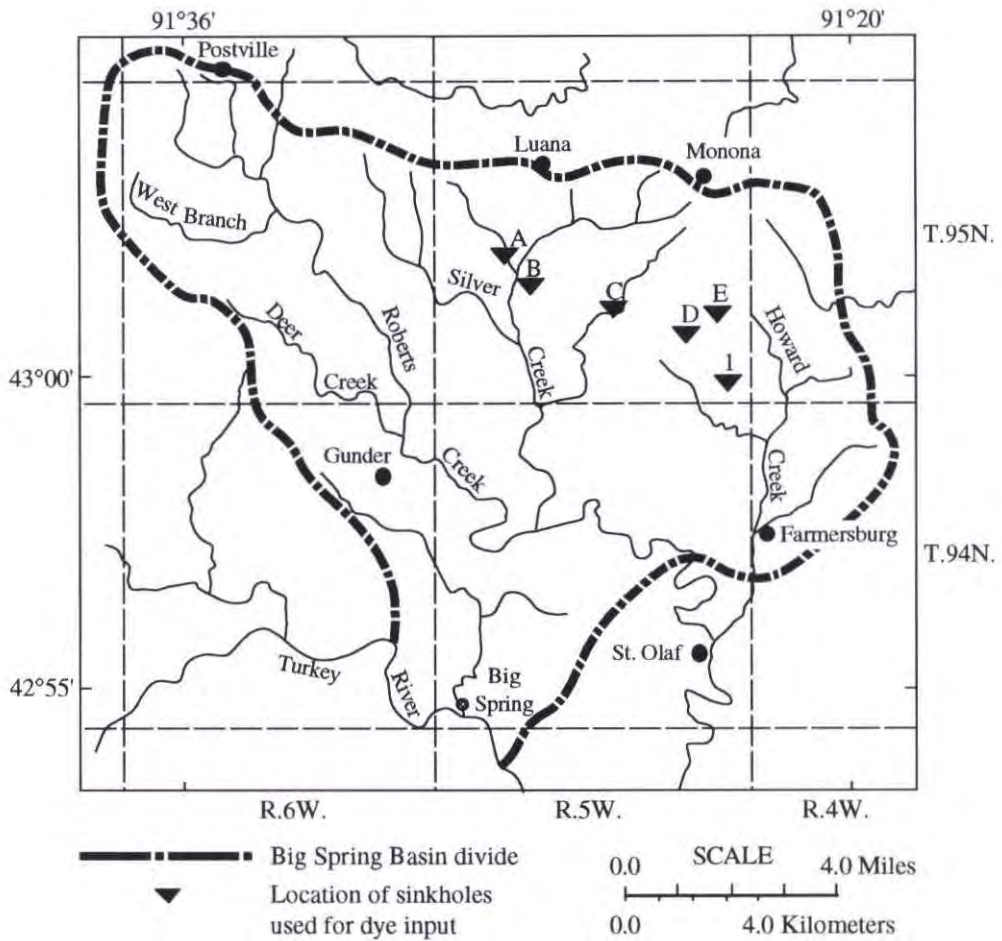


Figure 13. Location of Sinkholes Used for Dye Trace Experiments, after Hallberg et al. (1983)

To simulate dye trace A, it is first assumed that all sixteen sinkholes have the same inflow of 0.05 cfs, giving a total inflow of 0.8 cfs. This assumption is a very minor one, since total sinkhole inflow only constitutes 1.3% of the total discharge at Big Spring. The rest of the discharge is assumed to originate from the aquifer-matrix. This simulation is done by using the fixed megapore topology previously used in the sensitivity analysis, and by imposing discharge on the aquifer-matrix in the area surrounding the arbitrarily-chosen sinkholes 60, 66, 94, and 118 so that the discharge at Big Spring is within the range of 62 to 65 cfs. The model is run for megapore diameters, D , ranging from 5 to 10 ft; two values of megapore roughness, k_s , 30 and 20; and two values of hydraulic conductivity, K , 7.6×10^{-5} fps and 7.6×10^{-6} fps. At time $t = 6$ hrs, a pollutant concentration of 2000 units is imposed at sinkhole 60 so that a pollutant flux of 100 units enters the sinkhole. Sinkhole 60 is chosen to represent the sinkhole used in the actual dye trace A experiment since it is the nearest sinkhole in the computational network to the real one.

Figure 14 presents the results of the simulation for megapore diameter, D , ranging from 5 to 10 ft; megapore roughness, k_s , equal to 30; and hydraulic conductivity, K equal

to 7.6×10^{-5} fps. During the simulation, discharge at Big Spring is 63.8 cfs. Complete results are given in Table 1.

Table 1. Results of Simulation of Dye Trace A

Diameter (ft)	Travel Time (hrs)		
	$K = 7.6 \times 10^{-5}$ fps $k_s = 30$	$K = 7.6 \times 10^{-5}$ fps $k_s = 20$	$K = 7.6 \times 10^{-6}$ fps $k_s = 30$
5	28	28	27
6	36	36	34
7	45	45	43
8	55	55	53
9	67	67	63
10	79	79	75

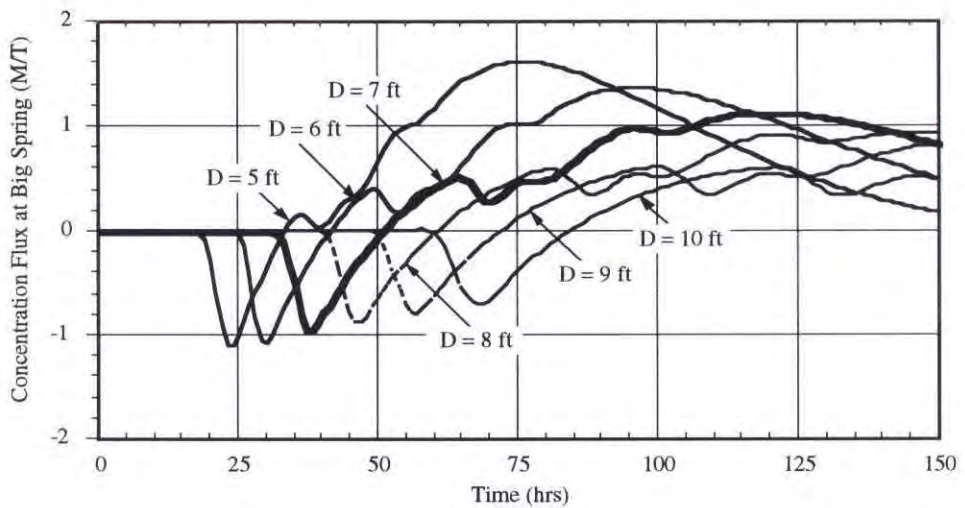


Figure 14. Results of Simulation of Dye Trace A for Several Megapore Diameters, D; Megapore Roughness, $k_s = 30$; and Hydraulic Conductivity, $K = 7.6 \times 10^{-5}$ fps

In Table 1, the travel times of the pollutant flux at Big Spring are taken to be the first positive pollutant flux encounters as shown in Figure 14. Figure 14 shows that due to numerical errors, negative pollutant flux precedes the first positive flux with the same order of magnitude. It should be realized that both the negative and positive pollutant fluxes are almost undetectable compared to the imposed pollutant influx of 100 units entering sinkhole 60.

Figure 14 and Table 1 show that, for all cases, a megapore diameter of 7 ft produces travel times that lie within the range of the real travel time of dye trace A; i.e., from 39 to 51 hours. Table 1 also shows that variation of megapore diameter gives significantly different travel times. Specifically, there is a narrow variation of megapore diameter that produces the correct travel time of dye trace A; i.e., about 1.25 ft or megapore diameters from 6.25 to 7.5 ft (see Figure 15). Table 1 shows that variation of megapore roughness, k_s , from 30 to 20 does not affect the travel time, while variation of hydraulic conductivity of the aquifer-matrix gives a difference of travel time ranging from 1 to 4 hours.

The second dye trace experiment simulated here was conducted on the Baade sink (trace 1, see Figure 13). The experiment began at 9:00 pm, when 2 pounds of Fluorescein dye were placed in a sinkhole on the Baade sink. At that time, a stream flow of 0.11 cfs was draining directly into the sinkhole, due to a heavy rain in the basin. Charcoal packets were replaced at 1/2 day intervals at Big Spring with the first dye appearing between 44 and 50 hours after input. Flow at Big Spring during this period was approximately 56 cfs (Hallberg et al., 1983).

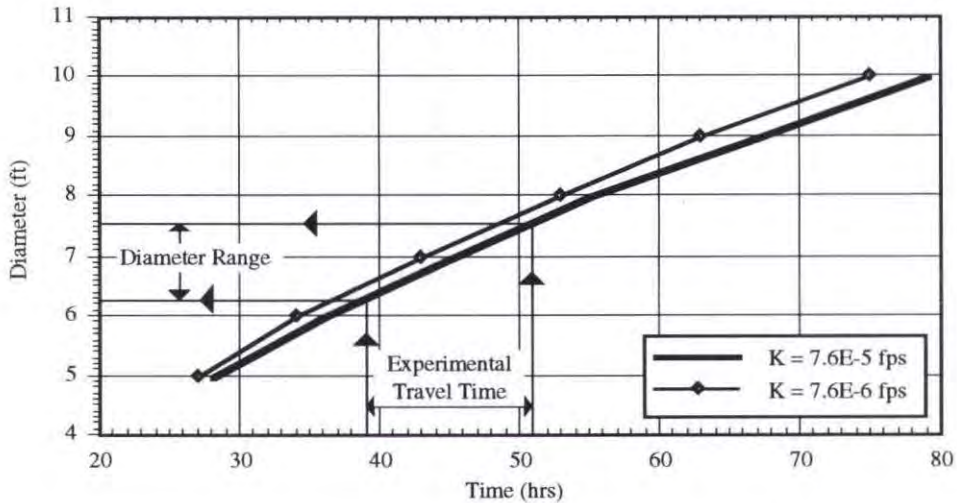


Figure 15. Travel Time, in Hours, versus Megapore Diameter, in Feet, in the Simulation of Dye Trace A

To simulate dye trace 1, it is first assumed that all sixteen sinkholes have the same inflow of 0.11 cfs, giving a total inflow of 1.67 cfs. This is a minor assumption since the sinkhole inflow only constitutes 3.0% of the total discharge at Big Spring. The rest of the discharge is assumed to originate from the aquifer-matrix. This simulation is done using the fixed megapore topology as before, and imposing discharge on the aquifer-matrix in the area surrounding sinkholes 25, 60, 66, and 112 so that the discharge at Big Spring is about 56 cfs. As in the previous dye trace experiment, these four sinkholes are chosen arbitrarily. The model is run for megapore diameters, D , ranging from 5 to 10 ft; two values of megapore roughness, k_s , 30 and 10; and two values of hydraulic conductivity, K , 7.6×10^{-5} fps and 7.6×10^{-6} fps. At time $t = 6$ hrs, a pollutant concentration of 2000 units is imposed at sinkhole 112 giving a pollutant flux of 220 units entering the sinkhole. Sinkhole 112 is chosen to represent the sinkhole used in the actual dye trace 1 experiment

since it is the nearest sinkhole in the computational network to the real one.

Figure 16 presents the results of the simulation for megapore diameter, D , ranging from 5 to 10 ft; megapore roughness, k_s , equal to 30; and hydraulic conductivity, K , equal to 7.6×10^{-5} fps. During the simulation, discharge at Big Spring is 56.0 cfs. Complete results are given in Table 2.

Table 2. Results of Simulation of Dye Trace 1

Diameter (ft)	Travel Time (hrs)		
	$K = 7.6 \times 10^{-5}$ fps $k_s = 30$	$K = 7.6 \times 10^{-6}$ fps $k_s = 30$	$K = 7.6 \times 10^{-6}$ fps $k_s = 10$
5	28	24	25
6	36	32	32
7	45	40	40
8	55	50	50
9	66	60	60
10	79	72	72

Figure 16 and Table 2 show that, for all cases, a megapore diameter of 7 ft produces travel times that lie within the range of the real travel time of dye trace 1; i.e., from 44 to 50 hours. Table 2 also shows that variation of megapore diameter gives significantly different travel times. Specifically, Table 2 shows that a narrow variation of megapore diameter produces the actual travel time of dye trace 1; i.e., about 0.6 ft or megapore diameters from 6.8 to 7.4 ft (see Figure 17). Table 2 shows that variation of megapore roughness, k_s , from 30 to 10 does not affect the travel time, while variation of hydraulic conductivity of the aquifer-matrix gives a difference of travel time ranging from 4 to 7 hours.

In Table 2, the travel times of the pollutant flux at Big Spring are taken to be the first positive pollutant flux encounters as shown in Figure 16. Figure 16 shows that due to numerical errors, negative pollutant flux precedes the first positive flux with the same order of magnitude. It should be realized that both the negative and positive pollutant fluxes are almost undetectable compared to the imposed pollutant influx of 220 units entering sinkhole 112.

Summary of Sensitivity Analysis and Dye Trace Simulations

This section summarizes the sensitivity analysis and dye trace simulations. From the results of the sensitivity analysis performed in previous sections, the parameters and megapore features affecting the Big Spring Basin can be ranked in order of importance, as presented in Table 3.

Table 3. Parameters and Features Affecting the Big Spring Basin

Parameter/Features	Degree of Importance
Megapore diameter	Very important
Diameter class	Very important
Hydraulic conductivity	Important
Megapore roughness	Important
Dispersion coefficient	Not important

It is important to mention that the above results are based on a fixed megapore topology. Presumably, megapore topology plays a more important role than megapore diameter. Moreover, the above results are based on following ranges of parameters: megapore diameter, D , from 3 ft to 30 ft; hydraulic conductivity, K , from 7.6×10^{-6} fps to 7.6×10^{-5} fps; megapore roughness, k_s , from 10 to 35; and Taylor dispersion coefficient, C_t , from 5.05 to 20.2, values which are 50% to 200% of the suggested value of C_t (10.1).

The results of sensitivity are summarized in the following paragraphs:

- (1) The size of the equivalent megapore dictates whether the overall system is responsive or diffusive. Generally, the smaller the diameter, the less responsive the system to a storm hydrograph entering sinkholes. Moreover, for a given megapore diameter, there is a threshold input hydrograph that the megapore can pass directly.
- (2) Megapore diameter classes are particularly important for pollutant transport while this feature does not significantly affect discharge response. The same discharge response at Big Spring may be obtained by replacing several megapore diameter classes by one uniform diameter, but it is difficult to get the same pollutant response using this procedure.
- (3) After megapore diameters and their classes, hydraulic conductivity of the aquifer-matrix is the third most important parameter. The importance of hydraulic conductivity is due to its contribution to the baseflow of the system. Generally, in any storm event, if there is pollutant in the water, the storm acts only as a carrier to bring the pollutant from outside into the system (i.e., aquifer-matrix and megapore network). Inside the system itself, the pollutant is usually carried by the baseflow, except for the case of small megapore diameters in which small amounts of the pollutant are also carried by the storm, resulting in a flashy downstream pollutant flux.
- (4) Megapore roughness is a mildly important parameter. Generally, this parameter only slightly affects the peak discharge of water and pollutant, as well as the time to peak. The overall behavior of responses at Big Spring is not affected by this parameter.
- (5) The dispersion coefficient also does not play an important role in the present study since the advective phenomenon is dominant compared to the diffusive one. Variation of the value of the dispersion coefficient, C_t , from 50% to 200% of the suggested value does not give significant differences in pollutant transport at Big Spring.

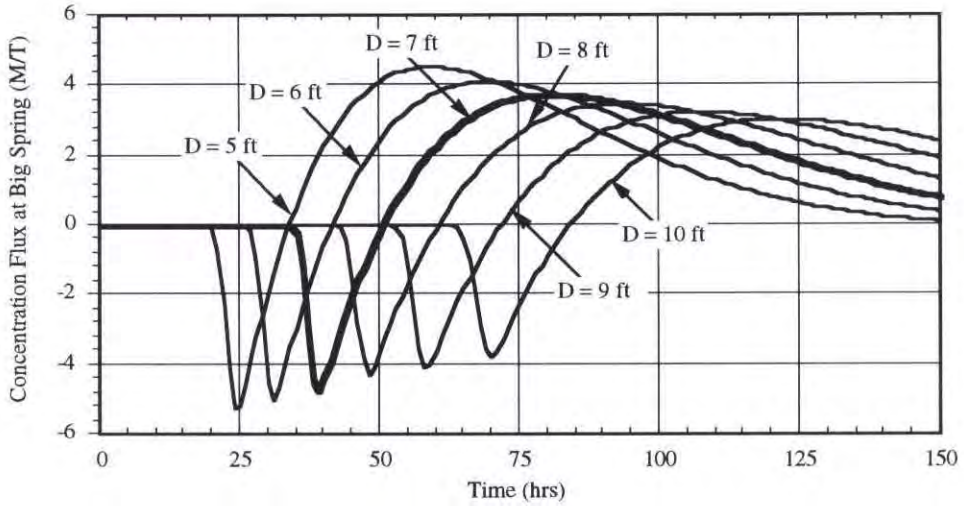


Figure 16. Results of Simulation of Dye Trace 1 for Several Megapore Diameters, D ; Megapore Roughness, $k_s = 30$; and Hydraulic Conductivity, $K = 7.6 \times 10^{-5}$ fps

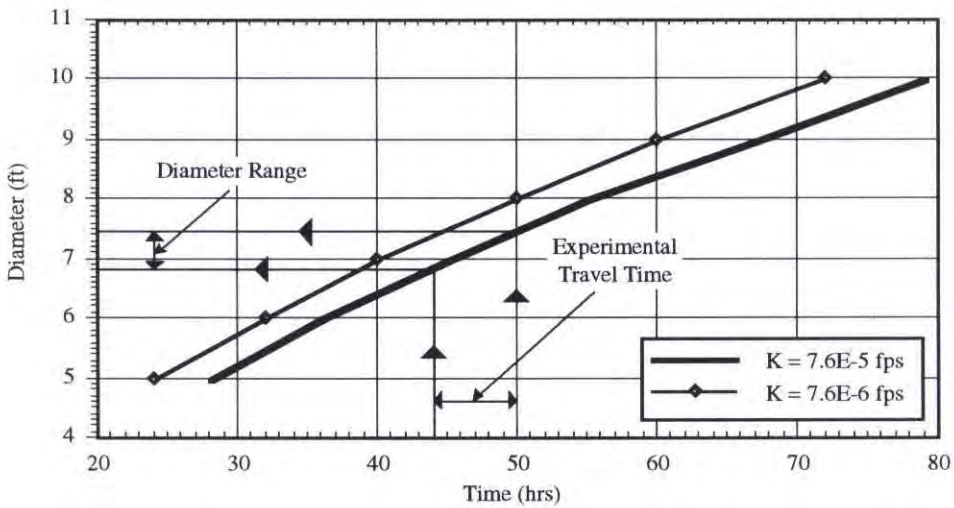


Figure 17. Travel Time, in Hours, versus Megapore Diameter, in Feet, in the Simulation of Dye Trace 1

Figure 18 shows that discharge response at Big Spring for a 20 ft megapore diameter, D , represents a conduit response in which most water flows through megapores, while D equal to 7 ft represents a diffuse response in which most water flows through the aquifer-matrix. This result agrees with the conceptualization of Hallberg et al. (1983), Figure 19, which shows the difference between conduit-flow and diffuse-flow in a carbonate aquifer.

The simulation of the dye trace experiments, shows that travel times of the dye traces are very sensitive to megapore diameter, confirming that megapore diameter is the most important parameter affecting the system. The range in magnitude of diameter that produces

the actual travel time is within 1.5 ft of the representative diameter. Even though the representative diameters chosen in the previous section are not necessarily the actual ones, the range of deviation from the representative diameter is an important finding. This narrow deviation shows that megapore diameter significantly affects pollutant transport. These results confirm the conclusion of the sensitivity analysis on megapore diameter.

The simulation results show that the maximum outflow at Big Spring usually coincides with a point in the inflow hydrograph. It should be possible, therefore, to predict the flow at Big Spring using a reservoir-type formulation, which avoids the complexity of a detailed mathematical formulation that considers all the water pathways (megapore network). For pollutant transport, however, the pathways are important and the reservoir formulation is not adequate to determine the concentration of pollutants in the Big Spring flow. Thus, the discharge response at Big Spring can be written as:

$$\frac{dO}{dt} = I(t) - O(t) \quad (67)$$

where $I(t)$ is known storm hydrographs entering sinkholes and $O(t)$ is discharge response at Big Spring. When $O(t)$ reaches maximum value, i.e., $\frac{dO}{dt} = 0$, the discharge response at Big Spring is $O(t = t_1) = I(t = t_1)$. As the system becomes a diffusive one, i.e., the megapore diameters decrease, Eq. (67) will no longer apply.

CONCLUSIONS

This section summarizes all results obtained from the present study. First, from sensitivity analysis, important parameters and features of the karst region have been identified. The most important parameter is the equivalent megapore diameter, and its distribution throughout the megapore network is the most important feature of the megapores. Other parameters affecting the Big Spring Basin ranked in order of importance are hydraulic conductivity of the aquifer-matrix, megapore roughness and dispersion coefficient. The megapore dispersion coefficient does not affect the basin, since the pollutant transport is dominated by advection rather than dispersion phenomenon.

Second, the main objective of the present study has been achieved by the computer code Labyrinth. The Labyrinth code is capable of simulating the behavior of saturated groundwater flow and pollutant transport in karst regions. The two modes of the flow; fast-response flow in cave passages and slow-response flow in the aquifer-matrix, have been correctly reproduced by the Labyrinth code.

Third, the results of the dye trace simulation, viewed in a Monte Carlo simulation framework, succeed in producing realizations for dye trace A and I experiments. Thus, the Labyrinth code has shown the capability to serve as a "deterministic engine."

FINAL REMARKS

As a part of a larger research objective — to serve as the deterministic engine of a Monte Carlo simulation of water resources in a karst region — the Labyrinth code has a promising future. At present, however, due to limited availability of data and time, the Labyrinth code can only produce the qualitative behavior of saturated groundwater flow

and pollutant transport. If more field data and resources become available in the future, more thorough tests can be performed on the Labyrinth code to completely understand its behavior and to calibrate parameters, thus enabling the present code to predict future conditions of the Big Spring Basin during wet seasons. Moreover, the extension of the Labyrinth code to handle unsaturated cases and its inclusion in a Monte Carlo simulation will make the code a powerful tool to analyze water resources in karst regions.

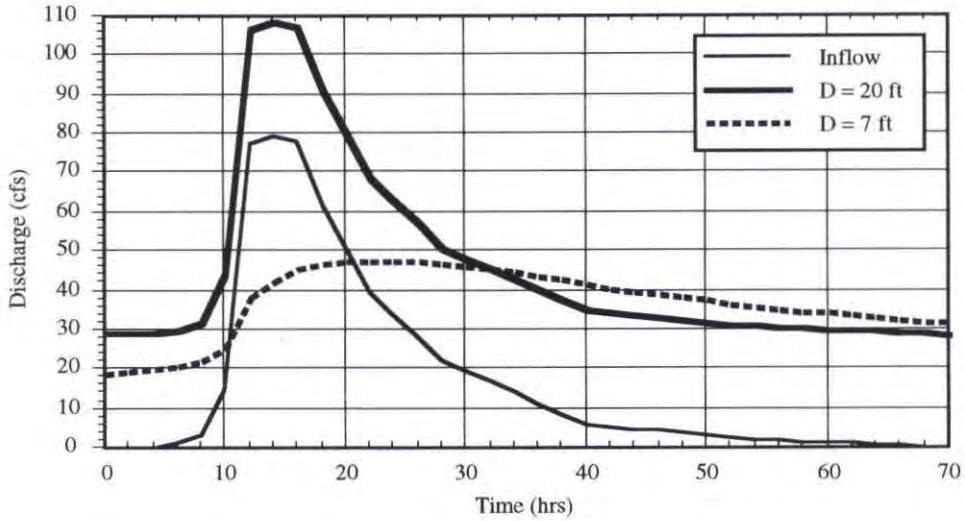


Figure 18. Discharge Hydrographs at Big Spring for Megapore Diameters, D, 7 ft and 20 ft.

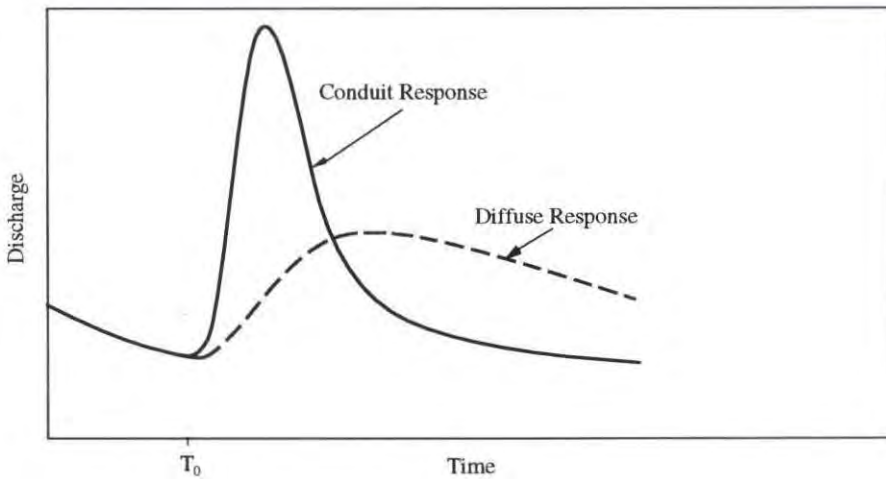


Figure 19. Schematic Hydrographs Showing the Difference between Conduit-Flow and Diffuse-Flow Discharge in a Carbonate Aquifer (e.g., at a spring) over Time, in Response to a Recharge Event at Time, T_0 , after Hallberg et al. (1983).

ACKNOWLEDGEMENT

This paper is a condensed version of Ph.D. dissertation supervised by Professor Forrest M. Holly Jr., The University of Iowa, Iowa 52242, USA.

REFERENCES

- Andersson, Johan and Dverstorp, Björn, (1987), Conditional Simulations of Fluid Flow in Three-Dimensional Networks of Discrete Fractures, Water Resources Research, Vol. 23, No. 10, pages 1876–1886.
- Avdagic, Izet, (1976), Determination of Flow Through Flooded Karst Poljes by Use of Poljes and Piezometric Boreholes Water Level, Karst Hydrology and Water Resources, Vol.1, pages (16–1) to (16–14), Water Resources Publications, Fort Collins, Colorado 80522, USA.
- Baecher, G. B. and Lanney, N. A., (1978), Trace Length Biases in Joint Surveys, Proceeding 19th U.S. Rock Mechanics Symposium, pages 56–65
- Bear, Jacob, (1972), Dynamics of Fluids in Porous Media, American Elsevier, New York, USA.
- Bear, Jacob, (1979), Hydraulics of Groundwater, McGraw-Hill Book Company, USA.
- Bear, Jacob and Berkowitz, Brian, (1983), Groundwater Flow and Pollution in Fractured Rock Aquifers, Developments in Hydraulic Engineering – 4, Chapter 4, Elsevier Applied Science, London and New York.
- Cacas, M. C., Ledoux, E., de Marsily, G., Tillie, B., Barbreau, A., Durand, E., Feuga, B., and Peaudecerf, P., (1990a), Modeling Fracture Flow With a Stochastic Discrete Fracture Network and Validation 1. The Flow Model, Water Resources Research, Vol. 26, No. 3, pages 479–489.
- Cacas, M. C., Ledoux, E., de Marsily, G., Barbreau, A., Calmels, P., Gaillard, B., and Margritta, R., (1990b), Modeling Fracture Flow With a Stochastic Discrete Fracture Network and Validation 2. The Transport Model, Water Resources Research, Vol. 26, No. 3, pages 491–500.
- Chow, Ven Te, Ph.D., (1959), Open-Channel Hydraulics, International Student Edition, McGraw-Hill International Book Company
- Cleary, R. W., and Unger, M. J., (1978), Groundwater Pollution and Hydrology, Mathematical Models and Computer Programs, Report 78–WR–15, Water Resources Program, Princeton Univ., Princeton, N. J.
- Cunge, J. A., Holly Jr., F. M., and Verwey, A., (1980), Practical Aspects of Computational River Hydraulics, Pitman Advanced Publishing Program, Boston • London • Melbourne.
- Dilamater, Ronald R. and Csallany, Sandor C., (1977), Hydrologic Problems in Karst Regions, Western Kentucky University, Bowling Green, Kentucky.
- Endo, H. K., Long, J. C. S., Wilson, C. R., and Witherspoon, P. A., (1984), A Model for Investigating Mechanical Transport in Fracture Networks, Water Resources Research, Vol. 20, No.10, pages 1390–1400.

- Feuga, Bernard, (1988), Modelling of Flow Through Fractured Rocks: Geostatistical Generation of Fracture Networks. Stress–Flow relationship in Fractures, Groundwater Flow and Quality Modeling, Editor: E. Custodio, A. Gurgui and J. P. Lobo Ferreira, NATO ASI Series, Series C: Mathematical and Physical Sciences Vol. 224, pages 269–297
- Fischer, Hugo B., List, E. John, Koh, Robert C. Y., Imberger, Jörg, and Brooks, Norman H., (1979), Mixing in Inland and Coastal Waters, Academic Press, Inc., Orlando, Florida 32887.
- Fujikawa, Yoko and Fukui, Masami, (1990), Adsorptive Solute Transport in Fractured Rock: Analytical Solutions for Delta-Type Source Conditions, Journal of Contaminant Hydrology, Vol. 6, pages 85–102.
- Haldeman, W. R., Chuang, Y., Rasmussen, T. C., and Evans, D. D., (1991), Laboratory Analysis of Fluid Flow and Solute Transport Through a Fracture Embedded in Porous Tuff, Water Resources Research, Vol. 27, No. 1, pages 53–65.
- Hallberg, G. R., Libra, R. D., Quade, D. J., Littke, B. and Nations, B., (1989), Groundwater Monitoring in the Big Spring Basin 1984–1987: A Summary Review, Energy and Geological Resources Division, Geological Survey Bureau, Technical Information Series 16, Iowa Department of Natural Resources.
- Hallberg, George R., Hoyer, Bernard E., Bettis III, E. Arthur, and Libra, Robert D., (1983), Hydrogeology, Water Quality, and Land Management in The Big Spring Basin, Clayton County, Iowa, Iowa Geological Survey, Open-File Report 83–3, Iowa City, Iowa 52242.
- Hallberg, George R., Libra, Robert D., Bettis III, E. Arthur, and Hoyer, Bernard E., (1984), Hydrogeologic and Water Quality Investigations in The Big Spring Basin, Clayton County, Iowa; 1983 Water-Year, Open-File Report 84–4, Iowa Geological Survey, Iowa City, Iowa 52242.
- Holly Jr., Forrest M. and Preissmann, Alexandre, (1977), Accurate Calculation of Transport in Two Dimensions, Journal of the Hydraulics Division, Vol. 103, No. HY11, pages 1259–1276.
- Iwai, K., (1976), Fundamental Studies of Fluid Flow Through a Single Fracture, Ph.D. Dissertation, University of California, Berkeley.
- Javandel, I., Doughty, C., and Tsang, C. F., (1984), Groundwater Transport: Handbook of Mathematical Models, Water Resources Monograph Series 10, American Geophysical Union, Washington, D.C.
- Kilbury, R. K., Rasmussen, T. C., Evans, D. D., and Warrick, A. W., (1986), Water and Air Intake of Surface-Exposed Rock Fractures in Situ, Water Resources Research, Vol. 22, No. 10, pages 1431–1443.
- Liggett, James A and Medina, Daniel, (1988), Flow in Three-Dimensional Fracture Networks Using a Discrete Approach, Groundwater Flow and Quality Modeling, Editor: E. Custodio, A. Gurgui and J. P. Lobo Ferreira, NATO ASI Series, Series C: Mathematical and Physical Sciences Vol. 224, pages 363–374
- Long, Jane C. S. and Billaux, Daniel M., (1987), From Field Data to Fracture Network Modeling: An Example Incorporating Spatial Structure, Water Resources Research, Vol. 23, No. 7, pages 1201–1216.
- Marcus, H., (1962), The Permeability of a Sample of an Anisotropic Porous Medium, Journal of Geophysic. Resources., 67, pages 5215–5225.
- Marcus, H. and Evanson, D. E., (1961), Directional Permeability in Anisotropic Porous

- Media, Contribution 31 Water Resources Center, University of California, Berkeley, page 105.
- Milanovic, Petar, (1976), Water Regime in Deep Karst. Case Study of the Ombla Spring Drainage Area, Karst Hydrology and Water Resources, Vol.1, pages (7-1) to (7-27), Water Resources Publications, Fort Collins, Colorado 80522, USA.
- Moreno, L., Neretnieks, I., and Eriksen, T., (1985), Analysis of Some Laboratory Tracer Runs in Natural Fissures, Water Resources Research, Vol. 21, No. 7, pages 951-958.
- Peck, Adrian, Gorelick, Steven, de Marsily, Ghislain, Foster, Stephen, and Kovalevsky, Vladimir, (1988), Consequences of Spatial Variability in Aquifer Properties and Data Limitations for Groundwater Modelling Practice, the International Association of Hydrological Sciences Publication No. 175, IAHS Press, Institute of Hydrology, Wallingford, Oxfordshire OX10 8BB, UK.
- Pollard, D. D., (1976), On the Form and Stability of Open Hydraulic Fractures in the earth's Crust, Geophysics Res. Letters, 3, no. 9, pages 513-516
- Robertson, A., (1970), The Interpretation of Geological Factors for Use in Slope Stability, Proc. Symposium on the Theoretical Background to the Planning of Open Pit Mines with Special References to Slope Stability, South African Institute of Mining and Metallurgy, Johannesburg, South Africa, pages 55-71
- Sauvaget, Patrick, (1982), Dispersion in Rivers and Coastal Waters — 2. Numerical Computation of Dispersion, Developments in Hydraulic Engineering – 3, Chapter 2, Elsevier Applied Science, London and New York.
- Schrauf, T. W. and Evans, D. D., (1986), Laboratory Studies of Gas Flow Through a Single Natural Fracture, Water Resources Research, Vol. 22, No. 7, pages 1038-1050.
- Sharp, J. C., (1986), Fluid Flow Through Fissured Media, Ph.D. Dissertation, Imperial College, London, 1986.
- Tsang, Y. W. and Tsang, C. F., (1987), Channel Model of Flow Through Fractured Media, Water Resources Research, Vol. 23, No. 3, pages 467-479.
- Tsang, Y. W., (1984), The Effect of Tortuosity on Fluid Flow Through a Single Fracture, Water Resources Research, Vol. 20, No. 9, pages 1209-1215.
- Usseglio-Polatera, J.M. and Chenin-Mordojovich, M.I., (1988), Fractional Steps and Process Splitting Methods for Industrial Codes, Developments in Water Science 36, Computational Methods in Water Resources, Vol. 2 Numerical Methods for Transport and Hydrologic Processes, Editors: Celia, M.A., et. al., pages 167-172
- Witherspoon, P. A., Long, J. C. S., Majer, E. L., and Myer, L. R., (1988), Combined Seismic and Hydraulic Method of Modeling Flow in Fractured Low Permeability Rocks, Groundwater Flow and Quality Modeling, Editor: E. Custodio, A. Gurgui and J. P. Lobo Ferreira, NATO ASI Series, Series C: Mathematical and Physical Sciences Vol. 224, pages 299-329